NOTICE

The quality of this microform is heavily dependent upon the quality of the original thesis submitted for microfilming. Every effort has been made to ensure the highest quality of reproduction possible.

If pages are missing, contact the university which granted the degree.

Some pages may have indistinct print especially if the original pages were typed with a poor typewriter ribbon or if the university sent us an inferior photocopy.

Previously copyrighted materials (journal articles, published tests, etc.) are not filmed.

Reproduction in full or in part of this microform is governed by the Canadian Copyright Act, R.S.C. 1970, c. C-30.

AVIS

La qualité de cette microforme dépend grandement de la qualité de la thèse soumise au microfilmage. Nous avons tout fait pour assurer une qualité supérieure de reproduction.

S'il manque des pages, veuillez communiquer avec l'université qui a conféré le grade.

La qualité d'impression de certaines pages peut laisser à désirer, surtout si les pages originales ont été dactylographiées à l'aide d'un ruban usé ou si l'université nous a fait parvenir une photocopie de qualité inférieure.

Les documents qui font déjà l'objet d'un droit d'auteur (articles de revue, tests publiés, etc.) ne sont pas microfilmés.

La reproduction, même partielle, de cette microforme est soumise à la Loi canadienne sur le droit d'auteur, SRC 1970, c. C-30.

Canada

Performance of M-ary QAM in a Line-of-Sight Multipath Fading Channel

Gia Minh Lieu

A Thesis

In

The Department

of

Electrical Engineering

Presented in Partial Fulfillment of the Requirements
for the Degree of Master of Engineering at
Concordia University
Montréal Québec Canada

March 1988

ISBN 0-315-41591-6

ABSTRACT

Performance of M-ary QAM in a Line-of-Sight Multipath Fading Channel

Gia Minh Lieu

M-ary quadrature amplitude modulation (M-ary QAM) is a modulation technique suitable to high capacity microwave transmission systems for its bandwidth efficiency. However, high level QAM is sensitive to multipath fading (MPF).

This thesis presents a method to evaluate the probability of symbol error for M-ary QAM under different fading conditions in digital microwave transmission systems. The calculation is based on a recent postulated probability density function to characterize different fading conditions. The filter partition in M-ary QAM is assumed to satisfy the optimum, intersymbol interference (ISI) free Nyquist criteria.

Illustrative results for 16, 64 and 256-QAM are also presented.

ACKNOWLEGEMENTS

I would like to express my deep gratitude to my thesis supervisor, Dr. Tho Le-Ngoc, for giving me the opportunity to work on this topic, and for his patient guidance during the preparation of this research.

I would also like to express my appreciation to Mr. Jorge A. Brana, for technical discussions and encouragements, and to Mr. Domenico Baronello for proof reading my thesis.

This work was supported by the National Research Council of Canada (NSERC) under grant number A5987, awarded to Dr. Tho Le-Ngoc.

Table of Contents

List of Figures

List of Table

List of Symbols

τ_a	Duration of fading activity
ξ	Fading activity Constant
d_a	Transmission path length in miles
c	Terrain factor
τ_m	Maximum delay between the direct and the reflected ray
$<\tau_{av}>$	Average delay estimation
$f_{\Theta}(\theta)$	Phase distribution of an MPF signal
$f_R(r)$	Amplitude distribution of an MPF signal
$I_0()$	Zeroth-order modified Bessel function
$\Gamma(m)$	Gamma function
$\phi_c(\tau)$	Autocorrelation function (time domain)
$\phi_c(\Delta f)$	Autocorrelation function (frequency domain)
$\phi_c(\Delta t)$	Spaced-time correlation function
$S_c(f)$	Doppler power spectrum
B_d	Doppler spread of the channel
$(\Delta t)_c$	Channel coherence time
β	Relative amplitude between the direct and the reflected ray
τ	Relative time delay between the direct and the reflected ray
$H(j\omega)$	MPF channel transfer function
$A(f)$	Attenuation response

f_r	Resonance frequency
C_i	Adaptive coefficient of an equalizer
d_k	k^{th} symbol decision
$x(t)$	Wide sense stationary uncorrelated scattering model
$d(t)$	Lowpass equivalent input signal
g	Nonnegative real constant
$b(t,\tau)$	Zero-mean complex Gaussian process
$P_r\left\{error/x\right\}$	Probability of error for a modulation technique
$f_X(x)$	Probability density function of x
$s(t)$	Transmitted signal
$n(t)$	Additive white gaussian noise
$r(t)$	Received signal
d_i	Bit stream
f_b	Bit rate
f_s	Symbol rate
$i(t)$	In-phase component of $\sqrt{M}$ -ary PAM or M-QAM
$q(t)$	Quadrature phase component of $\sqrt{M}$ -ary PAM or M-QAM
$I(t)$	Filtered signal of $i(t)$
$Q(t)$	Filtered signal of $q(t)$
$g_T(t)$	Transmitter filter response
$g_R(t)$	Receiver filter response
$p(t)$	Combined response of the transmitter and receiver filters.

$R(\omega,\alpha)$	Frequency domain of the raised-cosine pulse
$r(t,\alpha)$	Time domain of the raised-cosine pulse
P_{av}	Average power of $\sqrt{M}$ -PAM
σ_2	Variance of a Gaussian noise
P_T	Total Transmitted power
$P_{\sqrt{M}}$	Probability of symbol error of $\sqrt{M}$ -ary PAM
P_M	Probability of symbol error of M-ary QAM
E_s	Symbol energy of M-ary QAM
$i_{MPF}(t)$	In-phase component of M-ary QAM in an MPF channel
$q_{MPF}(t)$	Quadrature phase component of M-ary QAM in an MPF channel
$P_{\sqrt{M},MPF}$	Probability of symbol error of $\sqrt{M}$ -PAM in an MPF channel
$P_{M,MPF}$	Probability of symbol error of M-QAM in an MPF channel
B_i	Discret random variable

CHAPTER I

INTRODUCTION

1.1 Multipath Fading

Since the early 1970 's, microwave radio has become an important medium for digital communications. This tendency has been stimulated by the rapid development of digital technology. Microwave radio can provide the reliability and availability as other major communication systems, namely optical fiber and satellite systems. In addition, the major advantage of digital radio over optical fiber is its lower installation cost. Its primary advantage over satellite transmission is its smaller propagation delay [1]. However, microwave radio propagates in a natural medium in which anomalous propagation sometimes exist. This can cause a very severe degradation in radio system performance. This phenomenon has been referred to as multipath fading (MPF) [2,3].

The propagation mechanism that causes MPF in line-of-sight (LOS) transmission is shown in figure 1.1.

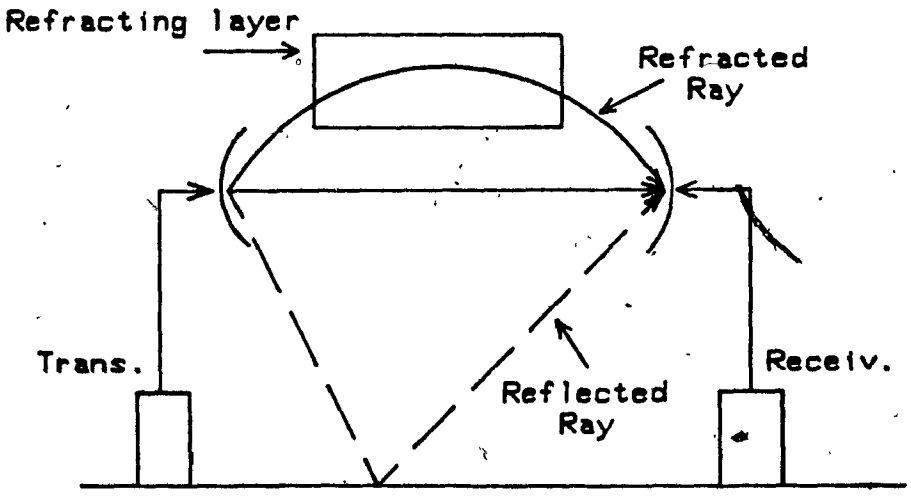

Figure 1.1 MPF phenomenon.

MPF is the destructive summation of multiple-electro-magnetic waves, with different wavelengths and phase angles, reaching to the receiving antenna via different paths. These interfering waves are the result of refraction and reflection due to both atmospheric and terrain conditions.

Refraction occurs in the atmosphere and is particularly obvious during a hot, calm and humid summer night. Under these conditions, normal atmospheric turbulence is minimal thus allowing tropospheric stratification with moisture distribution to occur, therefore, causing different refractive gradients in the atmosphere. Hence, a multiplicity of signal paths with different relative amplitudes and delay exist.

The reflected waves are caused by large surfaces : such as ground, bodies of water and the atmosphere. Other causes of MPF are due to meteorological phenomenon such as : rain, snow, fog, change of ions in the atmosphere and other factors. Hence, MPF is a function of path length, frequency, climate and terrain.

The severity of fading is depended on the relative amplitude of the reflected ray to that of the direct ray. There are two main fading conditions, deep fading and signal peaking. Deep fading occurs when the primary and secondary ray are equal in amplitude but opposite in phase thus resulting in a deep signal null. On the other hand, when the primary and secondary ray are equal in phase and amplitude, signal peaking occurs. Between these two extreme cases, other fading conditions exist. The various fading phenomenon are illustrated in figure 1.2.

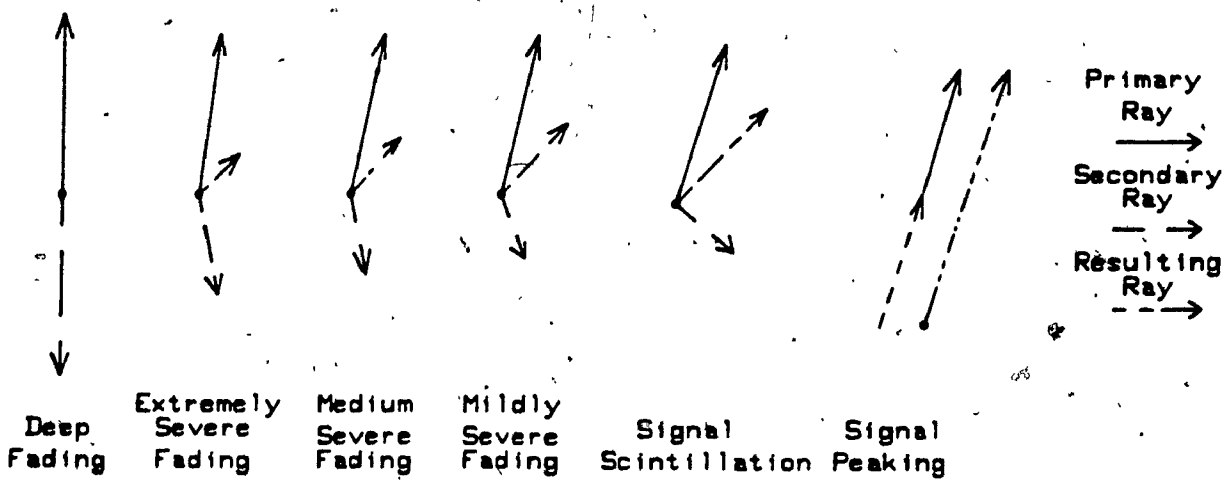

Figure 1.2 Vectors diagrams for various MPF effect.

When fading is caused by rain or snow, the attenuation shows no particular preference for any given frequency. This is known as frequency flat fading. However, the fade may be much higher at some frequencies and change more or less in a random fashion along the frequency axis. This phenomenon is known as frequency-selective fading. An example of the effect of frequency-selective fading is shown in Figure 1.3.

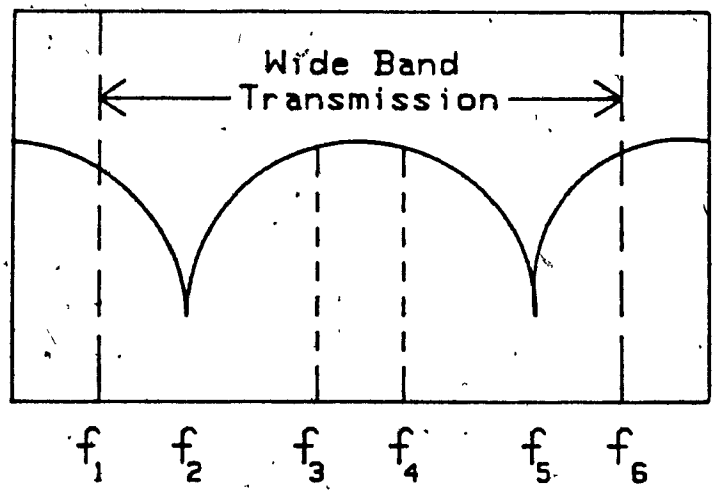

Figure 1.3 Effect of frequency selective fading.

Babler [4] has shown that as the transmission bandwidth increases, the distortion is more severe (see also figure 1.3). For narrow band transmission, the channel frequency response appears to be flat at f_3 and f_4. However, for the wide band transmission, channel response suffers selective fading at f_2 and f_5.

In an MPF channel, when the amplitude of the direct signal is stronger than that of the reflected signal, the amplitude and phase delay change in agreement. This condition is referred to as minimum phase, and is shown in figure 1.4a. On the other hand, when the reflected component is stronger than that of the direct signal, the phase delay varies opposite to the amplitude response. This case is known as the non minimum phase, and is shown in figure 1.4 b [3].

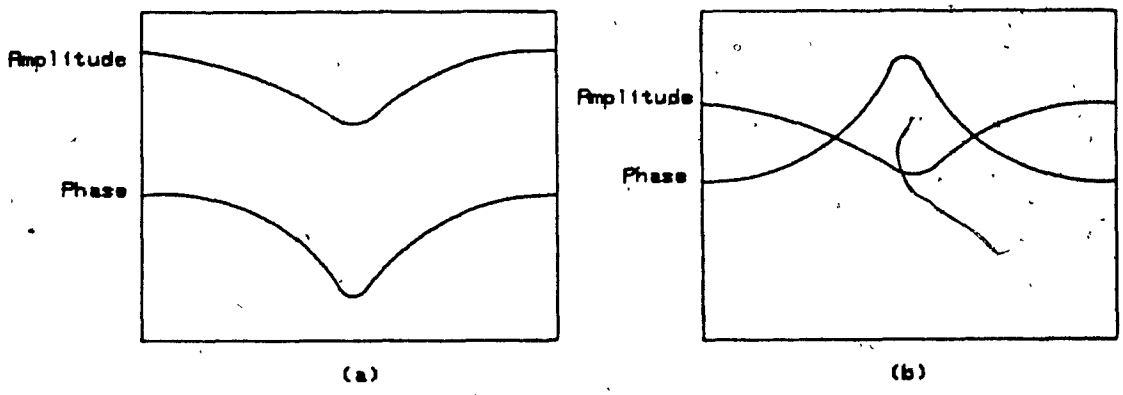

Figure 1.4 Minimum & non-minimum phase fading events

The phenomenon of MPF is temporary and random, however, it is a major cause of outage in microwave radio systems where high capacity transmission rate is used. In chapter II Various MPF characteristics and mathematical models will be investigated in detail.

1.2 Scope of The Thesis

The main objective of the thesis is to study the performance of M-ary QAM systems in a line-of-sight MPF channel. The main contributions of the thesis are :

* A general analysis for M-ary QAM in an MPF channel.

* The derivation of an explicit method to calculate the performance of M-ary QAM under various fading phenomenon based on a recent postulated probability density function (PDF) representing MPF.

Chapter I provides an introductory overview of the subject.

Chapter II is divided into four sections, starting with the characteristization of MPF. Secondly, different MPF models are investigated. In the third section, various countermeasuring techniques are discussed. The chapter then ends with a review of previous investigations of M-ary QAM in a fading channel by different researchers.

Chapter III investigates the performance of M-ary QAM in an AWGN and MPF channel. In the analysis, the filter partitions are assumed to satisfy the optimum ISI free Nyquist Criteria.

Chapter IV reviews of a recent postulated probability density function [5,6] used to analyze the MPF phenomenon. The explicit expressions for the symbol error rate of M-ary QAM under different fading conditions are then derived.

Chapter V contains the final conclusion, and suggestions for further research.

CHAPTER II

MPF : CHARACTERIZATION, MODELING AND COUNTERMEASURING

2.1 Characterization

In this section, some of the statistical characteristics of the channel will be briefly investigated. The section starts with an estimation of the fading activity. Next, a discussion of the MPF effect on the amplitude and phase is presented. Finally, the section ends with a quantitative treatment of the channel coherence bandwidth and coherence time.

2.1.1 Fading Occurrence Estimation

For very short paths, multipath fading seldom occurs. Ruthroff [7] defines a short path d_s in which no deep fading (more than -3 dB) occurs. However, for longer paths, deep fading has a dominant effect on the system response. Hence, an important parameter is the duration of the fading activity, and is given as

$$\tau_a = \xi c d_s f^3 \qquad (2.1)$$

where f : frequency in GHz

d_s : path length in miles

c : terrain factor

The terrain factor is defined as [8]

$$c = \begin{cases} 1 & \text{for } \textit{average terrain} \\ 4 & \text{for } \textit{over water} \text{ and } \textit{gulf coast} \\ 0.25 & \text{for } \textit{mountain} \text{ and } \textit{dry climate} \end{cases} \tag{2.2}$$

Based on experiments, Rummler [9] estimated ξ to be 0.073. However, based on the same experiment conditions, Greenstein and Czekaj [10] estimated ξ to be 0.11.

2.1.2 Relative Delay, Phase and Amplitude Distribution

(a) Relative Delay of The Reflections

Ruthroff [7] defined the maximum delay between the direct ray and the reflected ray as follows

$$\tau_m = 3.7 \left(\frac{d_s}{20} \right)^3 \tag{2.3}$$

where τ_m is given in nanoseconds and d_s is the path length in miles.

For a short path, the maximum delay is estimated as

$$\tau_m = \left(\frac{3}{8f} \right) \tag{2.4}$$

However, several researchers [11,12] prefer to use the average delay estimation, which is

$$<\tau_{av}> = 0.26\left(\frac{d_s}{20}\right)^3 \qquad (2.5)$$

(b) Phase Distribution $f_\Theta(\theta)$

Usually, an uniform distribution is assumed for the phase of the components of a multipath signal, that is [12]

$$f_\Theta(\theta) = \frac{1}{2\pi} \qquad 0 \leq \theta < 2\pi \qquad (2.6)$$

However, for a three-path model (see section 2.2), the phase distribution is different, namely [13]

$$f_\Theta(\theta) = \begin{cases} \frac{5}{6\pi} & |\theta| < \frac{\pi}{2} \\ \frac{1}{6\pi} & \frac{\pi}{2} \leq |\theta| < \pi \end{cases} \qquad (2.7)$$

(c) Amplitude Distribution

There are four probability density functions associated with the amplitude of the combined received multipath signal : the Rayleigh, Rice, Lognormal and Nakagami distributions.

The Rayleigh distribution is given by

$$f_R(r) = \left(\frac{r}{k^2}\right) \exp\left(-\frac{r^2}{2k^2}\right) \qquad r \geq 0 \tag{2.8}$$

The Rice distribution is given by

$$f_R(r) = \left(\frac{r}{K_2^2}\right) \exp\left(\frac{-(r^2 + k_1^2)}{2k_2^2}\right) I_0\left(k_1 \frac{r}{k_2^2}\right) \qquad r \geq 0 \tag{2.9}$$

where $I_0()$ is the zeroth-order modified Bessel function of the first kind.

The Lognormal-distribution is given by

$$f_R(r) = \left(\frac{1}{kr\sqrt{2\pi}}\right) \exp\left(\frac{(ln(r) - \mu_r)^2}{2k^2}\right) \qquad r \geq 0 \tag{2.10}$$

The Nakagami distribution is given by

$$f_R(r) = \left(\frac{2}{\Gamma}\right) \left(\frac{m}{\Omega}\right)^m r^{(2m-1)} \exp\left(-\frac{mr^2}{\Omega}\right) \qquad m \geq \frac{1}{2} \quad r \geq 0 \tag{2.11}$$

where $\Gamma(m)$ is the Gamma function, $\Omega = E[r^2]$, and $m = \dfrac{(E[r^2])^2}{Var[r^2]}$.

This general distribution reduces to various other known distribution for specific values of the parameter m (e.g., for the Rayleigh distribution for m = 1).

In a beyond-the-horizon transmission, the received signal approximately follows a Rayleigh distribution. While in a line- of-sight transmission, it approximately follows a Rice distribution. The Lognormal and Nakagami distributions are considered to give the best fit over longer distances (i.e., distance greater than several hundred miles). In addition, Aulin [14] has found that the Nakagami distribution gives the best fit of the data at the expense of mathematical complexity.

2.1.3 Channel Coherence Bandwidth

The range over which there is a significant correlation between two frequency components is called the coherence bandwidth of the channel. If the bandwidth of the transmitted signal is much less than the coherence bandwidth of the channel, then the channel appears to be frequency non-selective.

Suppose that a narrow pulse is transmitted at times t and $t + \tau$ .The autocorrelation function $\phi_c(\tau)$, of the channel is

$$\phi_c(\tau) = \frac{1}{2}E[h(t)h^*(t+\tau)] \qquad (2.12)$$

where $h(t)$ is the channel impulse response and the asterisk denotes the complex conjugate.

$\phi_c(\tau)$ can also represent the average output power of the channel as a function of τ. Hence, $\phi_c(\tau)$ is called " delay power spectrum " of the channel. This function is shown in figure 2.1 (a). The non zero value range is called the multipath spread of the channel and is denoted by τ_m.

An analogous characterization can also be done in the frequency domain $\phi_c(\Delta f)$. The transform relationship is

$$\phi_c(\Delta f) = \int_{-\infty}^{+\infty} \phi_c(\tau) e^{-j2\pi\Delta f \tau} d\tau \qquad (2.13)$$

As a result of Fourier transform between $\phi_a(\Delta f)$ and $\phi_c(\tau)$, the relation to the power spectrum can be expressed as

$$(\Delta f)_c = \frac{1}{\tau_m} \qquad (2.14)$$

where $(\Delta f)_c$ denotes the coherence bandwidth and is shown in figure 2.1 b.

When $(\Delta f)_c$ is smaller than the bandwidth of the transmitted signal, the radio system is frequency selective.

When $(\Delta f)_c$ is large than the bandwidth of the transmitted signal, the system is frequency non-selective.

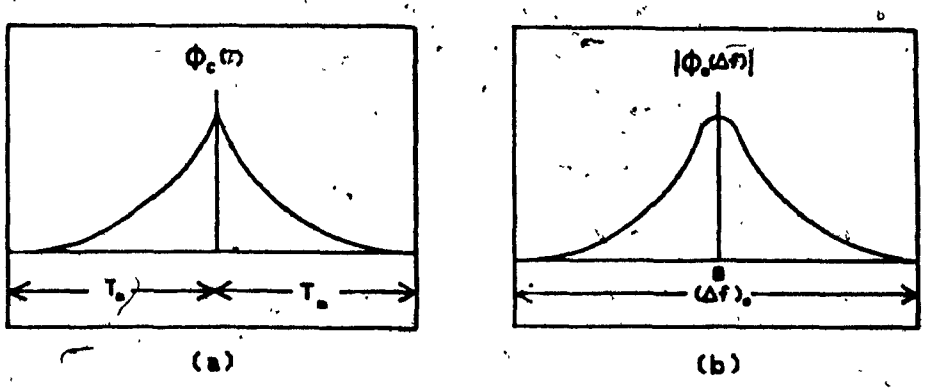

Figure 2.1 Channel coherence bandwidth.

(a) Delay power spectrum.

(b) Frequency correlation function

2.1.4 Channel Coherence Time

In digital transmission, 2^m waveforms are used to encode m bits. If the fading distortion remains constant during the transmission of one waveform (i.e., during a symbol interval) then the channel is a " slowly fading channel ". Otherwise it is a fast fading channel.

$\phi_c(\Delta t)$ is defined as a function to separate two sinusoids in time. $\phi_c(\Delta t)$ is equivalent to the correlation of a pure frequency tone with itself transmitted Δt seconds later. The Fourier transform of this function is $S_c(f)$

$$S_c(f) = \int_{-\infty}^{+\infty} \phi_c(\Delta t)\exp(-j\,2\pi f\,\Delta f)\,d(\Delta t). \qquad (2.15)$$

where $f = \frac{v}{\lambda}\cos\theta$, v is the relative velocity between the transmitted and reflected rays, and λ is the wavelength of the transmitted wave.

The range of values over which $S_c(f)$ is essential non-zero is called the Doppler Spread of the channel and is denoted by B_d.

Its reciprocal is an approximate measure of the coherence time of the channel

$$(\Delta t)_c = \frac{1}{B_d} \tag{2.16}$$

where $(\Delta t)_c$ denotes the coherence time and is given by the width of $\phi_c(\Delta t)$, as shown in figure 2.2.

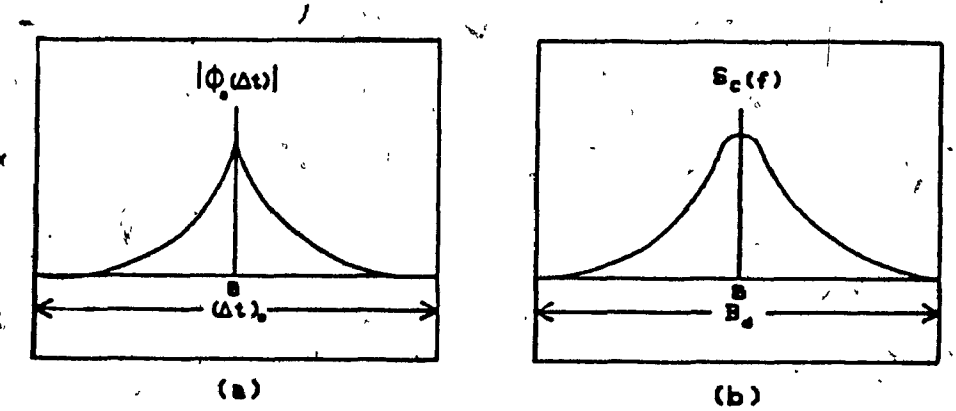

Figure 2.2 : Channel Coherence time

(a) Spaced-time correlation function

(b) Doppler power spectrum

If $(\Delta t)_c$ is large (relative to the duration of one information symbol), the channel is a slow fading channel.

If $(\Delta t)_c$ is relatively small and thus B_d relatively large, the channel is a fast fading channel.

2.2 Modeling

A MPF model transfer function, $H(jw)$, provides a mathematical fit of the propagation response over a finite bandwidth. The function $H(jw)$ contains a set of adjustable fitting parameters to approximate the dispersive channel response and predicts the fading signal amplitude.

In the following section, transfer functions of four models will be analyzed. The models are as follows : two-path model, three-path model, simplified three-path model; and the polynomial model.

2.2.1Two Path Model

The two-path model describes the multipath propagation in terms of a primary ray and a dominant interfering ray. It is assumed that all the reflected rays are combined into one reflected ray, and that the received signal is formed by the direct ray plus one reflected ray.

The time domain of the two-path model is given by [16]

$$r(t) = s(t) + \beta s(t-\tau) \tag{2.17}$$

The channel transfer function of this model is given by

$$H(jw) = 1 + \beta \exp(-j\omega\tau) \tag{2.18}$$

where β is the relative amplitude and τ is the relative delay between the reflected and the main rays.

The resultant diagram is shown in figure 2.3

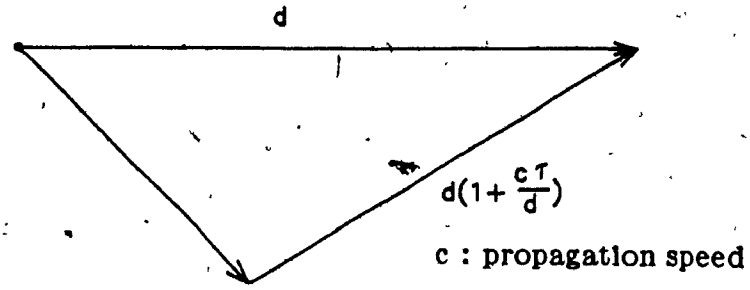

Figure 2.3 Vector diagram of a two-path model

In the two-path model, the direct ray is normalized to unity amplitude and zero phase, and the reflected ray has an amplitude β and relative phase angle $\theta = \omega\tau$. Both β and τ are statistically independent random variables.

The amplitude of the combined signal is given by

$$L = (1 + \beta^2 + 2\beta\cos\omega\tau)^{1/2} \tag{2.19}$$

The phase of the combined signal is given by

$$\phi = \tan^{-1}\left(\frac{\beta \sin\omega\tau}{1+\beta\cos\omega\tau}\right) \tag{2.20}$$

The power transfer function of the channel is given by

$$|H(w)|^2 = 1 + \beta^2 + 2\beta\cos\omega\tau \tag{2.21}$$

The envelop delay is in turn given by

$$T(w) = \frac{d_\omega \phi}{d\omega} = \frac{\beta(\beta + 2\cos\omega\tau)}{1+\beta^2+2\beta\cos\omega\tau} \tag{2.22}$$

The deepest fading occurs at

$$\omega_b \tau = 2\pi\left(n - \frac{1}{2}\right) \tag{2.23}$$

The two-path model is mathematically simple, yet it is able to feature the effect of frequency selective fading, as shown in the typical amplitude response plot in figure 2.4.

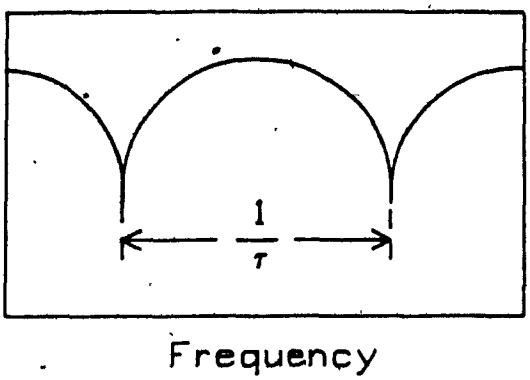

Figure 2.4 Typical amplitude response of a two-path model.

The two-path model has been most often used to analyze the effect of MPF. This is due to its simplicity and because frequency selective fading is usually the dominant cause of system outage for high capacity radio systems. However, some accuracy is obviously sacrificed by adopting this model.

2.2.2 General Three-Path-Model

For analysis purposes, the MPF channel has been modeled by the two-path criteria. However, some investigators [4,9] have maintained that the two-path model is not sufficient. The time domain representation of the three-path model is

$$r(t) = s(t) + \beta_1 s(t - \tau_1) + \beta_2 s(t - \tau_2) \qquad (2.24)$$

The channel transfer function for a three-path model is given by

$$H(j\omega) = 1 + \beta_1 \exp(-j\omega\tau_1) + \beta_2 \exp(-j\omega\tau_2) \qquad (2.25)$$

where 1 is the normalized amplitude of the direct ray and β_1 and β_2 represent the normalized amplitudes of two reflected rays. With respect to the direct ray, the second and third rays are delayed by τ_1 and τ_2, respectively, where $\tau_2 > \tau_1$. The vector representation of this model is shown in figure 2.5.

However, this model is seldom used due to its mathematical complexity. Most investigators prefer to use either the two-path model, or the simplified three-path model as described in the next section.

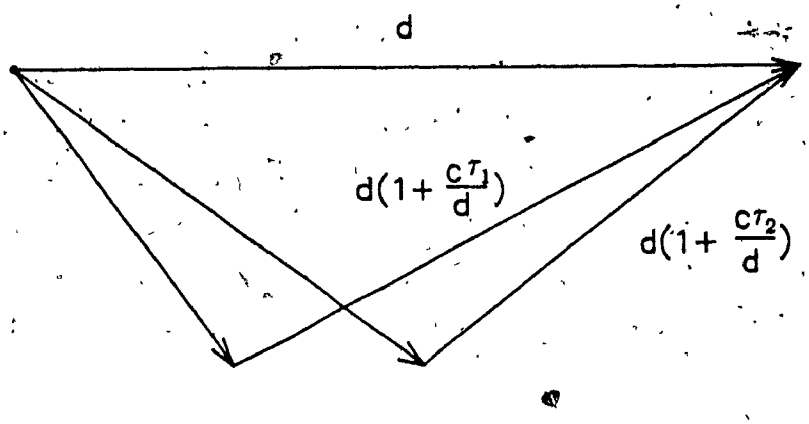

Figure 2.5 Vector diagram of a three-path model

2.2.3 Simplified Three-Path Model

The simplified three-path model was introduced and developed by Rummler [9]. With this model, all propagation responses over the bandwidth of interest are represented by a suitable choice of its adjustable parameters [17].

The transfer function of a simplified three-path model is given by

$$H(j\omega) = a\,[1 - \beta e^{-j(\omega - \omega_0)\tau}] \tag{2.26}$$

where the positive real parameters a and β control the scale and shape of the fade respectively, ω_0 is the notch frequency, and τ is the relative delay of the channel. In practice, the absolute value of τ is chosen to be six times the measurement bandwidth or 6.3 ns.

The relative amplitude β ranges from zero to one ($0<\beta<1$). The response is minimum phase when the sign of the delay is positive, and it is non minimum phase when the sign of the delay is negative. The non-minimum phase state is also obtained when the relative amplitude of the delayed ray is greater than unity ($\beta>1, \tau>0$).

The simplified three-path model is an useful tool for understanding the characterization of line-of-sight microwave radio channels. It also provides a good fit to almost all measured responses of a narrow band radio channel [9].

The amplitude of the combined signal is given by

$$L = a\,[1 + \beta^2 - 2\beta\cos(\omega - \omega_0)\tau]^{1/2} \tag{2.27}$$

The phase of the combined signal is given by

$$\phi = \tan^{-1}\left[\frac{\beta\sin\omega\tau}{1 - \beta\cos\omega\tau}\right] \tag{2.28}$$

The power transfer function of the channel is given by

$$|H(w)|^2 = a^2[1 + \beta^2 + 2\beta\cos((\omega - \omega_0)\tau)] \tag{2.29}$$

While the envelope delay is given by

$$T(\omega) = \frac{d\phi}{d\omega} = \frac{\beta(\cos((\omega - \omega_0)\tau)\beta)}{1 + \beta^2 - 2\beta\cos((\omega - \omega_0)\tau)} \tag{2.30}$$

2.2.4 Polynomial Model

In a narrow band transmission system, it is generally not possible to distinguish the time delays in the MPF channel. The alternative is then to fit the measured frequency transfer function into a polynomial series with the coefficients that closely approximates the MPF channel response.

The polynomial representation used for MPF is [17]

$$H(j\omega) = A_0 + \sum_{n=1}^{N} (A_n + jB_n)(j\omega)^n \tag{2.31}$$

The A_n and B_n coefficients vary with the effect of MPF upon the digital radio system.

In the first order complex polynomial model, the minimum phase condition corresponds to $A_1/A_0>0$, and the non-minimum phase corresponds to $A_1/A_0<0$.

The polynomial model may lead to simple methods for analyzing signal processing (note that $(j\omega)^n$ corresponds to the n-th derivative) and suggests the form of an adaptive equalizer response.

Other investigators have also suggested a different polynomial modeling [18,19], based on the attenuation response $A(f)$ of the MPF channel as

$$A(f) = \sum_{i=0}^{n} a_i f^i \tag{2.32}$$

where coefficients a_i 's have been obtained by using least square fitting. For most fading periods, polynomials of order m=2 are used. The second order polynomial is able to provide accuracy, familiarity, and simplicity. In addition, the impact of channel defects, amplitude, slope and parabolic distortion on equipment performance is easily measured and quantified using the second order polynomial [17]. For extremely severe fading events, the most suitable polynomial order is $M = 4$.

To determine whether the MPF channel encounters minimum or non-minimum phase fading, both amplitude and phase responses at a particular given time must be examined.

2.2.5 Selection Criteria

In the above analysis, the most commomly used MPF models have been presented. It has been shown that MPF models can be classified as a power series model (polynomial) or a path delay model (two-path, three-path, and simplified three-path).

In wide-band transmission, frequency-selective fading is a serious problem. Under this condition, it may be more desirable to use a power series representation to approximate the frequency response of the channel.

In narrow-band transmission, path-delay models are generally chosen. This is because they are more directly associated with the physical channel and are more convenient for statistical modeling of the parameters.

In practice, path-delay models are preferred, since the dominant effects are due to two or three paths only (that is, the direct ray plus one or two reflections). Of the path delay model, the two-path model has become the most popular model for investigating the effect of MPF, where only marginal accuracy is sacrificed.

2.3 Countermeasuring

To achieve high capacities in a microwave radio system, a high level modulation scheme must be used. In chapter III, one such modulation scheme QAM will be introduced. It will be shown that MPF causes ISI and crosstalk which degrade the system performance. Currently, there are three major methods to maintain

reliable transmission in an MPF environment. They are diversity, equalization, and forward error control coding (FEC). These MPF countermeasuring techniques will be discussed in the following sections.

2.3.1 Diversity

Diversity is used to improve the performance of a line-of-sight microwave radio. In diversity, redundant communication channels are used so that when one of the channels encounters fading, transmission is still possible over the remaining channels. Two popular diversity techniques are space diversity and frequency diversity.

Space diversity is implemented by using vertically spaced antennas at the receiver. It has been observed that with sufficient spacing between antennas, the fading effect of the received signal at one antenna tends to be independent of the other antenna. Space diversity can be realized by different techniques such as combining and switching.

Frequency diversity is implemented by setting aside one or more back up channels with different carriers and switching one of them into service when fading causes an outage in the working channel. Unlike space diversity, frequency diversity utilizes the switching technique only. The detail of switching and combining diversity will be discussed in the following sections.

(a) Switching Diversity

This diversity approach involves switching from one channel to another to obtain the strongest output at each instant.

In switching diversity, the channel, with the strongest signal output, is selected during MPF. This process will generally reduce the fade depth that would be observed with either signals alone. The general block diagram of switching diversity is shown in figure 2.6.

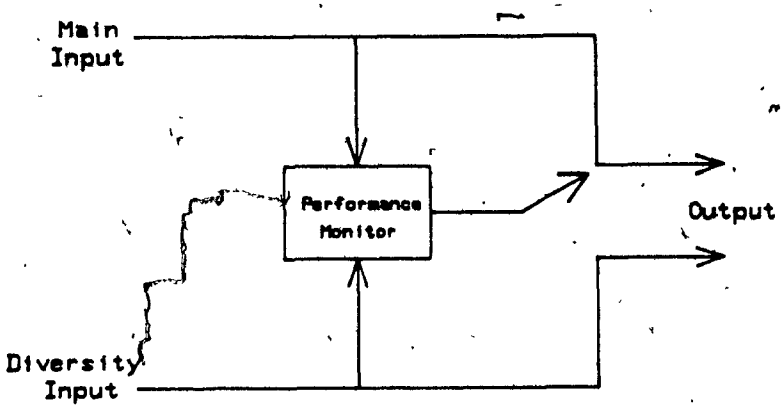

Figure 2.6 Block diagram of switching diversity.

The performance monitor compares the main and the diversity signals and through the switch, it provides the output with the best signal.

However, this approach requires automatic delay alignment to correct the different delay introduced by multipath.

2.3.2 Combining Diversity

The general block diagram of a combiner is shown in Figure 2.7. The basis operation principle is that the received signals from the main and diversity antenna are adaptively phase adjusted and then combined.

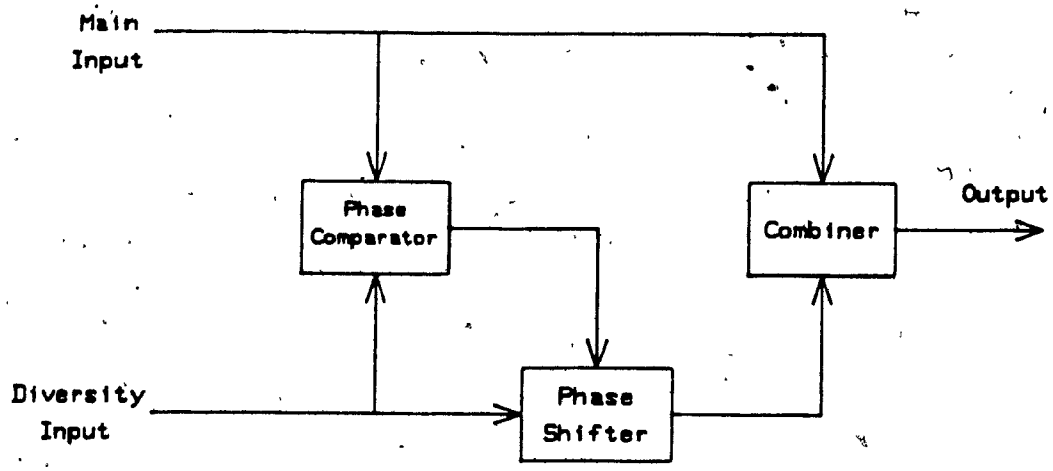

Figure 2.7 Block diagram of combing diversity.

There are two types of combining techniques and the details of each technique will be presented in the following.

The first approach is the maximum power combiner. It vectorally adds the output from the main and diversity antennas to give the maximum power output signal. This is done by shifting the main signal to be in phase with the diversity signal prior to combining the two signals [3].

The second approach is the minimum-distortion combiner. It functions similarly to the maximum-power unit but incorporates a different control approach for the phase shifter. When the signals of both antennas encounter multipath dis-

distortion, the phase of the main signal is rotated, to force the vector sum of the two signals to produce a flat output spectrum [3].

2.3.2 Frequency Domain Equalizer

The basic idea of a frequency-domain equalizer is to equalize the distortion in overall channel amplitude response. Two types of frequency domain equalizers, a slope equalizer and a notch equalizer, will be discussed in the following.

(a) Slope Equalizer

A general block diagram of a slope equalizer is shown in figure 2.8

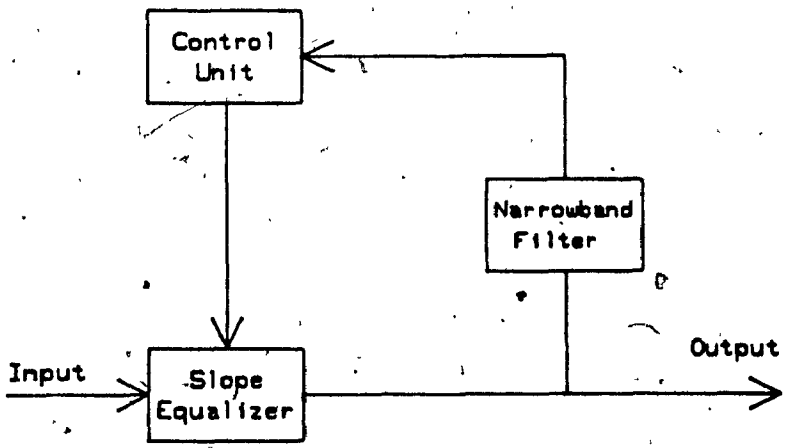

Figure 2.8 Block diagram of a slope equalizer.

The control unit detects the narrow band spectrum levels of the transmitted signal at three frequency f_{-1}, f_0, and f_{+1}, and the slope equalizer provides the approximate correction.

In the frequency domain, MPF often introduces slope asymmetries in the radio channel response (Figure 2.9 a).

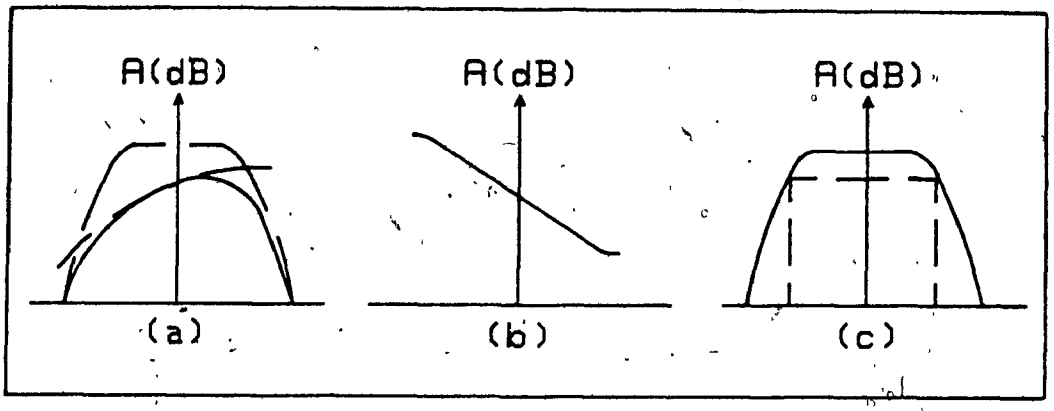

Figure 2.9 Spectrum correction with a slope equalizer

The function of the slope equalizer is to provide an amplitude tilt correction (Figure 2.9 b) which restorts equality to the spectral density (Figure 2.9 c). In addition, a slope equalizer is able to compensate for a frequency-selective fade where the amplitude attenuation lies outside the passband. Usually, a slope equalizer is designed with a flat group delay characteristic.

(b) Notch Equalizer

The function of the notch equalizer is to approximate the inverse amplitude and frequency delay characteristics of the channel. A general block digram of a notch equalizer is shown in Figure 2.10.

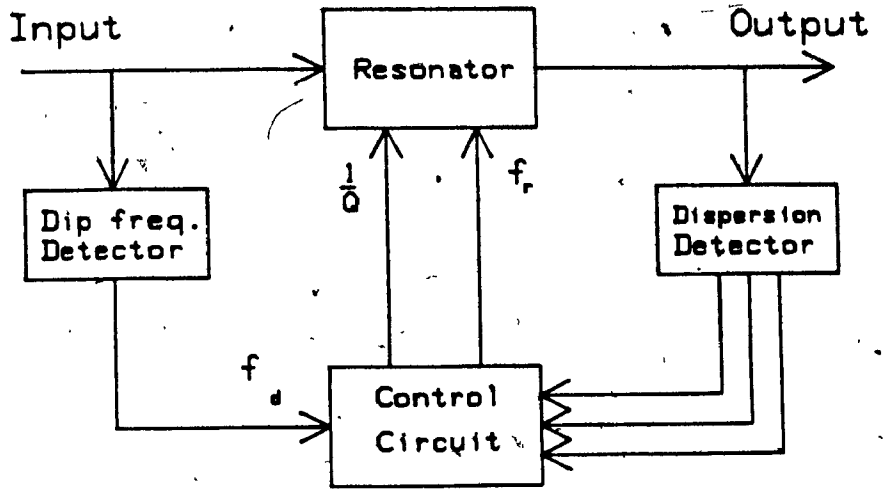

Figure 2.10 A notch equalizer.

A notch equalizer uses a variable resonator whose frequency response can be adjusted to correct the amplitude dispersion caused by MPF. The resonance frequency f_r and selectivity $1/Q$ of the resonator are controlled so as to make the overall amplitude response flat by detecting the narrow spectrum levels of transmitted signal at three frequencies [20]. Figure 2.11 illustrates the fade notch and the equalizer response.

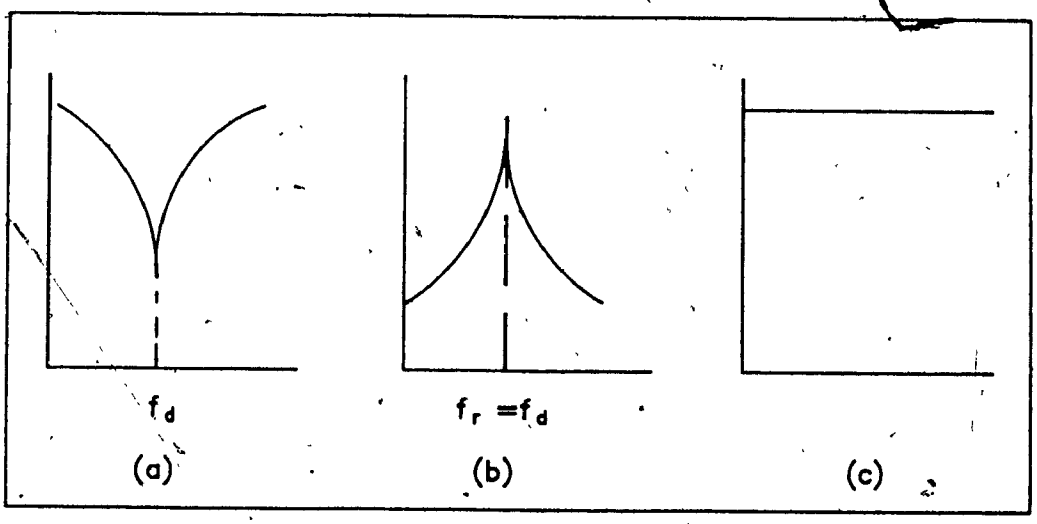

Figure 2.11 Spectrum correction with a notch equalizer.

2.3.3 Linear Transversal Equalizer

The general block diagram of a linear equalizer is shown in Figure 2.12.

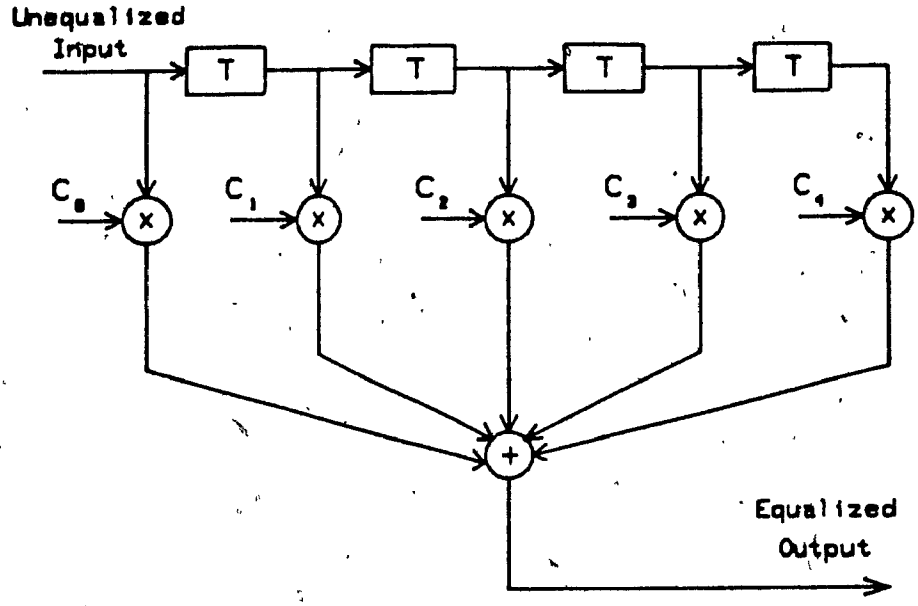

Figure 2.12 Linear transversal equalizer

The ability of a linear equalizer to control ISI is determined by the number of delay-line taps and the position of the reference tap at which the symbol is located. In practice, only a finite number of taps (usually 5 or 7) is required to compensate the effect of MPF. The center tap is usually chosen to be a reference tap so as to give equal effectiveness against distortion from both minimum and non-minimum phase fading.

The algorithm to adjust the tap gain is based on the zero-forcing (ZF) or minimum mean square error (MMSQ) principle. These two techniques lead to rather simple implementation, as required by high rate transmission. However, when the channel suffers severe fading distortion, the equalizer compensation can only be achieved by increasing the number of taps. In addition, to ensure the

convergence of the control algorithm, a non zero signal energy is required over the entire transmit band. This is obtained only if a signal scrambler is used [22].

(a) Zero Forcing (ZF) Technique

The general output of the transversal equalizer is

$$S(k) = \sum_{i=0}^{m} a_i r(k - i) \tag{2.33}$$

where m is the number of the equalizer coefficients.

In an ZF equalizer, the coefficients a_i are chosen to force the samples of the combined channel and the equalizer impulse response to zero at all but one of the NT instants. The effect of an ZF equalizer is shown in Figure 2.13 [23].

However, the tap convergence of the ZF equalizer is not guaranteed if the transmitted data are severely distorted. In addition, ZF equalizer ignores the effect of additive noise and interference due to the symbols outside the equalizer.

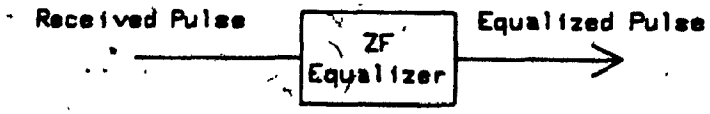

(a) Block diagram of an ZF equalizer

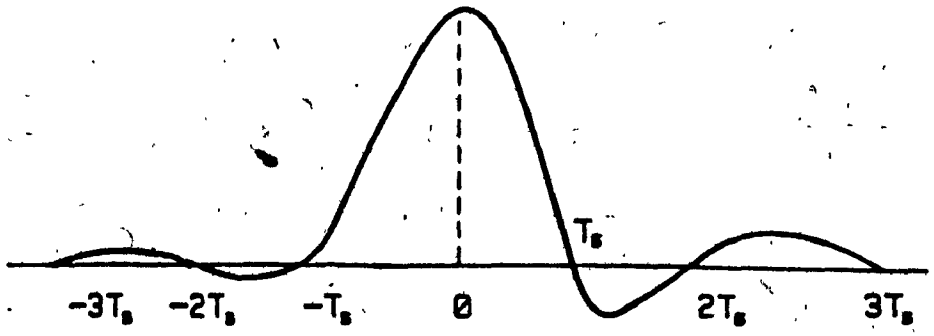

(b) Unequalized pulse

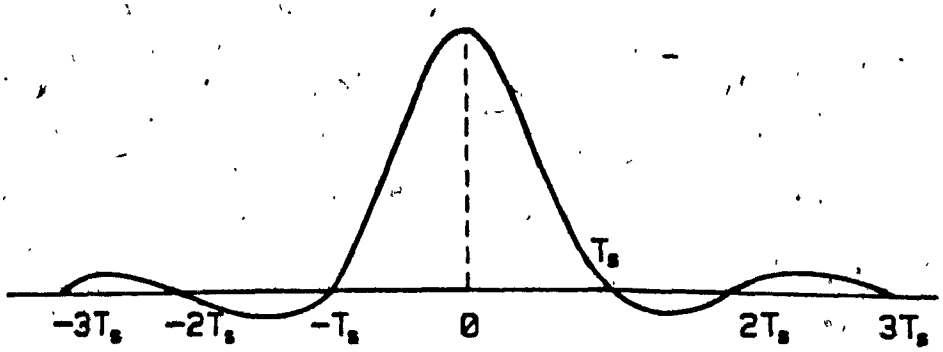

(c) Equalized pulse

Figure 2.13 The effect of an three tap ZF equalizer

(b) Minimum Mean Square Error (MMSE)

The tap gain coefficients of a MMSE equalizer are chosen to minimize the mean square error at the equalizer output, which is defined as the sum of ISI plus the additive noise power at the output of the equalizer.

The adjustment of the tap gains is involved during each symbol interval. It is in a direction opposite to an estimate of the gradient of the mean square error with respect to that of the tap gain [21]. Therefore, the set of equalizer coefficients will be closer to the optimum set corresponding to MMSE. As mentioned earlier, the output response of a transversal equalizer is

$$s(k) = \sum_{i=0}^{m} a_i \, r(k - i) \tag{2.34}$$

If d(k) is the desired response, and e(k) is the error between the output and the desired responses, the expectation of $|e(k)|^2$ is given by

$$E[|e(k)|^2] = E\left[\sum_{i=0}^{m} a_k \, r(k - i) - d\left(k - i\left(\frac{m}{2}\right)\right)^2\right] \tag{2.35}$$

To obtain the minimum variation of the mean square error against the tap weights, the following condition must be obtained, namely

$$\frac{\partial E[|e(k)|^2]}{\partial a_i} = 0 \qquad \text{for } all \ a_i \tag{2.36}$$

This results in a set of 2(m+1) linear equations. The solution of these equations gives the least mean square result [24]. Furthermore, since the mean square error is a quadratic function of the tap gains, convergence is always guaranteed independent of the noise or the interference.

2.3.4 Decision Feedback Equalizer

Decision feedback (DF) equalizer is a nonlinear equalizer. It uses a decision feedback to cancel the interference from symbols which have been detected. The DF equalizer is particularly useful for channels with severe amplitude distortion. The general block diagram of DF equalizer is shown in figure 2.14.

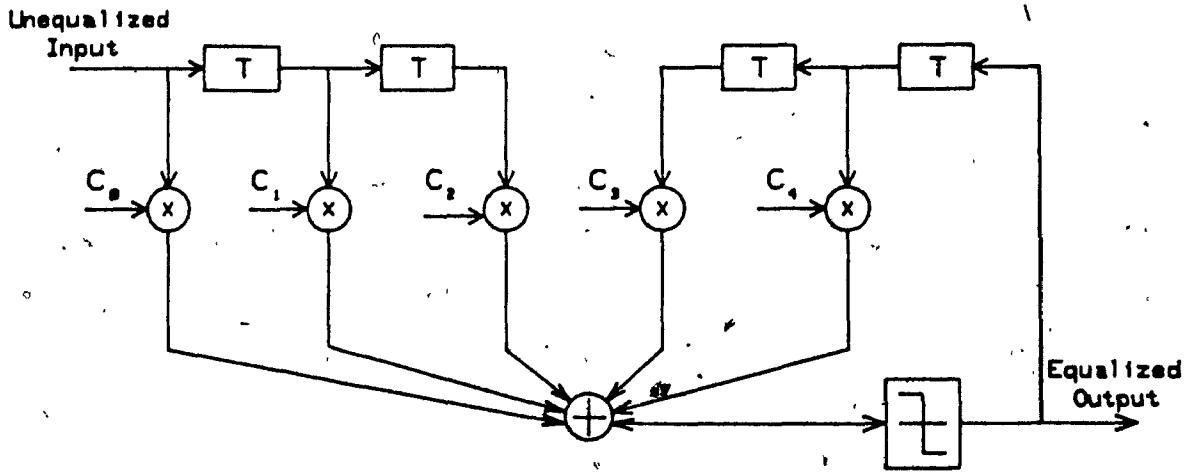

Figure 2.14 Adaptive decision feedback equalizer.

The equalizer contains two sections, a feedforward section and feedbackward section. The equalizer output is the sum of the outputs of the feedforward and feedbackward sections of the equalizer. The forward and backward coefficients may be adjusted simultaneously to minimize the mean square error.

The feedforward section is identical to the linear transversal equalizer.

The feedbackward part feeds back the output equalized signal via a second transversal filter. The basic idea is that if the value of the symbols already detect are known (past decisions are assumed to be correct), then the ISI contributed by these symbols can be canceled exactly. This is done by subtracting the past symbol values with approximate weighting from the equalizer output. The coefficients are adjusted according to

$$C_i\,(k\,+\,1) = C_i(k) - \nabla e_k\, d_{k\,-\,i} \qquad i\,=\,1,\ldots\ldots,m \qquad (2.37)$$

where d_k is the k^{th} symbol decision, $C_i(k)$ is the i^{th} feedback coefficient at time k and there are m coefficients at all.

2.3.5 Forward Error Correction (FEC) Coding

FEC coding is an efficient technique to correct severe distortions due to MPF. A general block diagram of a modulator/demodulator (modem) including the FEC scheme is shown in Figure 2.15.

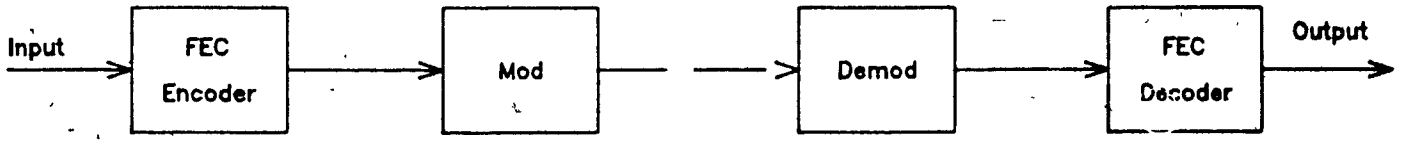

Figure 2.15 Block diagram of a modem with FEC.

The principle of FEC coding is to provide redundant information in the transmission system. Hence, it allows for a better detection and correction of errors at the expense of transmission bandwidth. For high spectral efficiency requirements long and high rate codes can be used at the expense of decoding complexity. As a result, FEC coding has not been widely used to correct the MPF effect.

2.3.6 Summary of Various Countermeasuring Techniques

So far, the countermeasuring techniques most commonly used to compensate the fading distortion have been presented. It has been shown that these techniques can be classified as diversity, equalization and FEC. These MPF correction techniques usually operate at baseband or intermediate frequency, because they are relatively easy to incorporate into the existing equipment.

Space diversity is the most commonly used countermeasuring technique. Desipte its simplicity, space diversity cannot adequately correct the in band dispersion caused by MPF, since the interfering rays cannot always be cancelled out [20]. Therefore, the improvement factor is relatively small and inadequate. In practice, space diversity is usually used in conjunction with some form of equalization.

Frequency diversity requires additional receivers and corresponding transmitters at the appropriate alternative frequencies. Hence, it reduces the number of active channels that can be accommodated in a given frequency.

The slope and notch equalizers are realized in the frequency domain. These two equalizers are generally considered to be simple, low cost countermeasuring

techniques. However, their performance under field trial experiments are not very impressive [21].

Zero forcing, minimum mean square, and decision feedback equalizers are realized in the time domain.

The ZF equalizer is widely used in microwave applications. This is due to the simplicity of its implementation where its tap gain updating circuitry can be implemented with logic gates.

The weights of MMSE equalizer converge more rapidly and minimizes both ISI and additive noise at the equalizer output. Although, the performance of MMSE equalizer is superior to the ZF equalizer, it is not used very often in practice due to the complexity of its control algorithm.

The DF equalizer is a non linear equalizer. Depending on the number of past symbols, a flexible choice of feedback coefficients can eliminate the ISI. However, the DF equalizer requires a high carrier to noise ratio to avoid incorrect decision which will perturb the weight convergence. In addition, during the transition between minimum and non minimum phase fading, the equalizer must calculate a new set of weight values. This introduces a severe step discontinuity in a long delay multipath.

The performance of each type of equalizer is influenced by the channel characteristics, as well as the actual number of coefficients and the position of the reference or main tap of the equalizer.

It is concluded that each countermeasuring technique has its advantages and disadvantages. The designer will have to choose a particular or a combination of the MPF countermeasuring techniques to achieve the transmission objectives.

2.4 A Survey of Previous Works on MPF

There exists an abundance of literature which discusses the performance of M-ary QAM in a MPF environment. The data published in these works, be it from mathematical analysis or from experiments, were evaluated in a protected system. That is to say, countermeasuring techniques were used in the analysis of the system performance. Unlike the other works, the results obtained in this thesis is for an unprotected system. In addition, since little work has been done in the system performance analysis of an unprotected system, the results of this work may be used as a reference when comparing performance improvement using countermeasuring techniques. In the following section, different performance evaluation methods which are readily applied to M-ary QAM will be discussed.

Hummels and Ratcliffe [25] developed a procedure to evaluate the error probability for an O-QPSK system operating in a MPF environment. In this work, a matched filter is assumed to be used. The received signal components contain a direct signal, a reflected signal and AWGN. fepresented by their equivalent complex envelope. The numerical evaluation of the probability of symbol error is facilitated by using Fourier series representations for both the signal-pulse function and the fading process. For both series, the expressions are truncated to the range [-N, 1] where N is a positive integer. The error probability is then given by the expression $P[r>0]$ where r contains the desired signal, noise, ISI due to the filtering process and MPF. Both ISI and Doppler effects are taken into account.

The procedure can be adopted for various digital modulation schemes. The performance of M-ary QAM systems can be evaluated by multiplying the results by the corresponding probabilities representing the M-levels. However, the computation is complicated. In addition, Rayleigh fading was assumed. This assumption is acceptable for mobile communication systems in the urban area. For microwave radio systems operating in the line-of-sight transmission. This assumption is not always true.

Milstein *et al* [26] presented an alternative method to calculate the performance of 16-QAM over a frequency selective Rician fading channel. In this analysis, the demodulator was assumed to have perfect carrier and symbol synchronization, which has been made in practice. The model used is the so-called wide sense stationary uncorrected scattering model (WSSUS) which has the following representation

$$x(t) = \mathrm{Re}\left\{ [d(t) + g\int_{-\infty}^{+\infty} b(t,\tau) d(t-\tau) d\tau] \right\} \qquad (2.38)$$

where $d(t,\tau)$ is the lowpass equivalent input signal, $b(t,\tau)$ is a zero-mean complex Gaussian process and g is a nonnegative real constant. In the demodulator, the received signal contains the desired signal, AWGN, and crosstalk from adjacent channels. According to the analysis, the 16-QAM contains a large alphabet size and hence makes the computation of the average probability of error very time consuming. Hence, instead of computing the average probability of error, a "worst-case" probability of error for a given point in the signal constallation would be found. This provides more pessimistic results than the real situation. In addition, this analysis does not provide a simple closed form solution.

In the last two decades, different methods to evaluate the probability of error for different digital modulation schemes in an MPF channel have been proposed. Most of these performance evaluations applied to the non coherent FSK and DPSK [27,28]. In general, different approaches have been used for each modulation technique, and depending on the complexity of detection, different assumptions have been made. A performance evaluation method based on these criteria seems to concentrate on a particular MPF channel. It fails to provide a general insight of the problem. Furthermore, for M-ary QAM, only a very limited amount of literature has referred to the system performance without MPF correction techniques.

In this thesis, a method to calculate the probability of symbol error for M-ary QAM has been proposed and will be presented. In this approach, the two-path model has been used to study the effect of MPF. It is assumed that all reflected rays are combined into one reflected ray, and that the received ray is formed by the direct ray plus one reflected ray. By applying the two-path model to describe the fading situation, only marginal accuracy has been sacrificed. In addition, the filter partition in the M-ary QAM system is assumed to satisfy the optimum ISI free Nyquist criteria which is an acceptable assumption in digital radio design.

The average error probability is calculated as

$$P_r = \int_{-\infty}^{+\infty} P_r \left\{ error / x \right\} f_X(x)\, dx \qquad (2.39)$$

where

$P\{error/x\}$ is the error probability of a modulation technique under an AWGN environment, and a given condition of x.

$f_X(x)$ is the probability density function of x which represents MPF.

The PDF $f_X(x)$ has been recently postulated by Brana and Le-Ngoc [5,6]. The condition of MPF changes with relative amplitude and phase of the reflection with respect to the direct signal. These two effects are integrated into a single parameter λ represent different fading conditions.

Evaluation of equation (2.39) can lead to a simple closed form solution. This method is flexible and general, since the same treatment can be applied to different kinds of digital modulation techniques.

CHAPTER III

PERFORMANCE OF M-ARY QAM SYSTEMS IN AN MPF CHANNEL

PART I : GENERAL ANALYSIS

3.1 Performance Analysis of M-ary QAM in an AWGN Channel

A general communication system model is used to study the performance of M-ary QAM (Figure 3.1). In this model, the transmission system is assumed to be distorted only by the additive white Gaussian noise (AWGN).

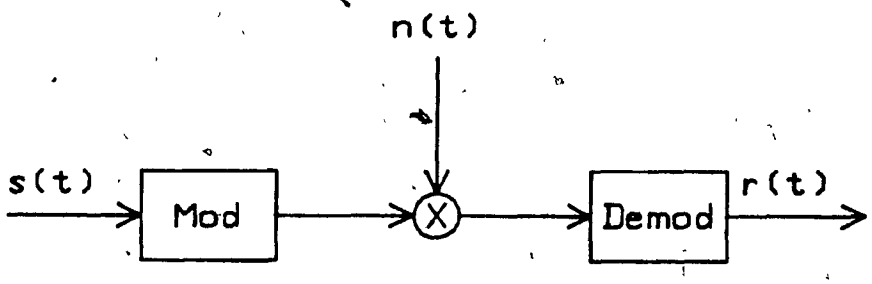

Figure 3.1 Block diagram for an AWGN communication system.

3.11 M-ary QAM Modulator

A block diagram for an M-ary QAM modulator is shown in Figure 3.2. The input to the M-ary QAM modulator is a bit stream d_i at rate f_b. This bit stream is fed to a serial-to-parallel converter to produce two parallel binary streams, in-phase and quadrature phase, at rate $f_{b/2}$. For each binary stream, an n-bit digital to analog (D/A) converter converts an n-bit sequence into an $\sqrt{M}$ -level pulse amplitude modulation signal ($\sqrt{M}$ -ary PAM) $i(t)$ *or* $q(t)$. The transmission rate of the $\sqrt{M}$ -ary PAM signal is $f_s = f_b/2n$. The in-phase and quadrature $\sqrt{M}$ -ary PAM signals, $i(t)$ and $q(t)$ are then filtered by two identi-

cal lowpass filters to shape the transmitted spectrum. The filtered signals, $I(t)$ and $Q(t)$ can be represented as

$$I(t) = d \sum_i a_i g_T (i - iT_s) \tag{3.1}$$

$$Q(t) = d \sum_i b_i g_T (t - iT_s) \tag{3.2}$$

where $T_s = \frac{1}{f_s} = \frac{2n}{f_b}$ is the symbol interval.

$a_i, b_i \in \{ \pm 1, \pm 3, \ldots, \pm(\sqrt{M} - 1) \}$ are the amplitudes with equal probability $\frac{1}{\sqrt{M}}$.

and $g_T(t)$ is the impulse response of the lowpass filter.

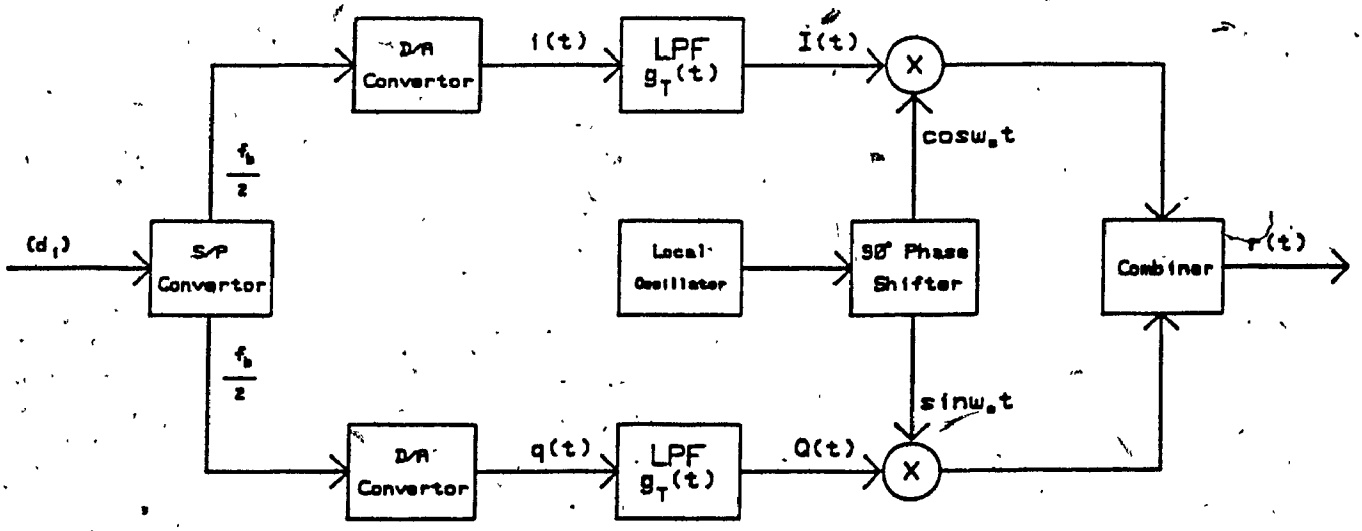

Figure 3.2 M-ary QAM modulator.

The filtered outputs $I(t)$ and $Q(t)$ are multiplied by $\cos\omega_c t$ and $\sin\omega_c t$ respectively, and then summed together to produce the M-ary QAM signal.

$$s(t) = I(t)\cos\omega_c t + Q(t)\sin\omega_c t \qquad (3.3)$$

where ω_c is the carrier frequency.

3.1.2 M-ary QAM Demodulator

The received signal to the M-ary QAM demodulator is

$$r(t) = s(t) + n(t) \qquad (3.4)$$

where $s(t)$ is given in equation (3.3), n(t) is the AWGN and is represented as

$$n(t) = n_I(t)\cos\omega_c t + n_Q(t)\sin\omega_c t \qquad (3.5)$$

where $n_I(t)$, and $n_Q(t)$ are the in-phase and quadrature Gaussian noise with the spectral density of $N_0/2$

The block diagram of an M-ary QAM demodulator is shown in Figure 3.3.

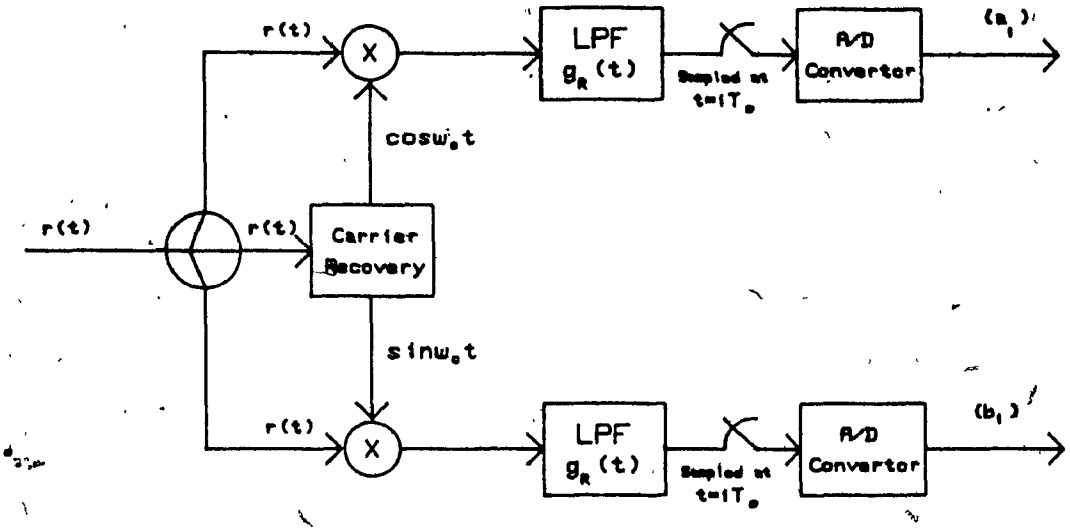

Figure 3.3 M-ary QAM demodulator.

A coherent demodulator structure is assumed. The recovery circuit produces $\cos\omega_c t$ and $\sin\omega_c t$. The received signal $r(t)$ is multiplied by $\cos\omega_c t$ and $\sin\omega_c t$, and then filtered by two identical lowpass filters respectively. From equations (3.1) to (3.5), the resulting signals are $i(t)$ and $q(t)$.

$$i(t) = I'(t) + n'_I(t) \tag{3.6}$$

$$q(t) = Q'(t) + n'_Q(t) \tag{3.7}$$

Where

$$I'(t) = [d\sum_i a_i\, g_R(t - iT_s)] * g_R(t)$$

$$= d\sum_i a_i\, p(t - iT_s) \tag{3.8}$$

$$Q'(t) = [d\sum_i b_i\, g_R(t - iT_s)] * g_R(t)$$

$$= d\sum_i b_i\, p(t - iT_s) \tag{3.9}$$

$$p(t) = g_T * g_R(t) \tag{3.10}$$

$$n_I'(t) = n_I * g_R(t) \tag{3.11}$$

$$n_Q'(t) = n_Q * g_R(t) \tag{3.12}$$

$i(t)$ and $q(t)$ are sampled at time $t = iT_s$ and then quantized by the A/D converters to reproduce the estimated value of $\{a_i\}$, and $\{b_i\}$.

3.1.3 Filter Partition

For zero ISI at the sampling instant $t = iT_s$, the impulse response $p(t)$ must satisfy the following condition [27].

$$p(iT_s) = \begin{cases} 1 & \text{if } i = 0 \\ 0 & \text{if } i \neq 0 \end{cases} \tag{3.13}$$

where I is an integer.

Then the resulting M-ary QAM signal $s(t)$ can be represented in a constellation diagram as shown in Figure 3.4 where M equals 16.

con

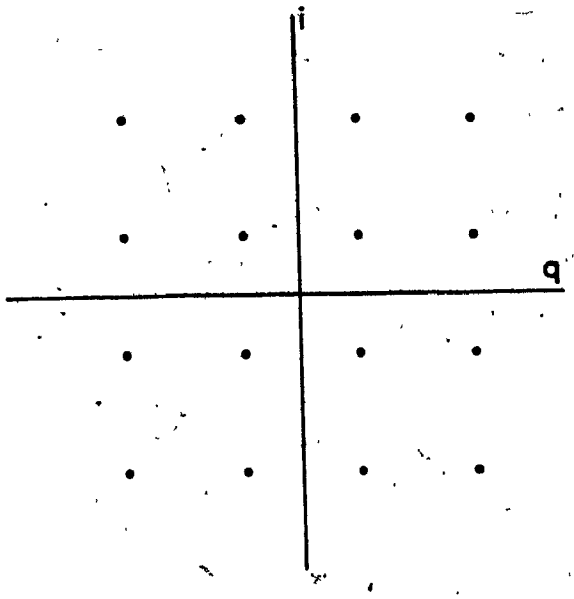

Figure 3.4 Constellation diagram of 16-QAM.

The condition for the optimum transmission is

$$|G_T(w)| = |G_R(w)| = \sqrt{R(w,\alpha)} \tag{3.14}$$

where $G_T(w)$ and $G_R(w)$ are frequency domain representation of $g_T(t)$ and $g_R(t)$ respectively, and are both assumed to have linear phase.

$R(w,\alpha)$ is the raised cosine filter. Its frequency domain characteristic is given by

$$R(w,\alpha) = \begin{cases} T_s & \text{if } 0 \le w \le \frac{\pi}{T_s}(1-\alpha) \\ \frac{T_s}{2}\left\{1 - \sin\left[\frac{T_s}{2\alpha}\left(w - \frac{\pi}{T_s}\right)\right]\right\} & \text{if } \frac{\pi}{2T_s}(1-\alpha) \le w \le \frac{\pi}{2T_s}(1+\alpha) \end{cases} \tag{3.15}$$

where α is the roll-off factor.

The time domain representation of the raised cosine filter is

$$r(t,\alpha) = \frac{\sin\pi t/T_s}{\pi t/T_s}\,\frac{\cos\alpha\pi t/T_s}{1-4\alpha^2 t^2/T_s^2} \tag{3.16}$$

Some of the raised cosine characteristics and their impulse responses are shown in Figure 3.5.

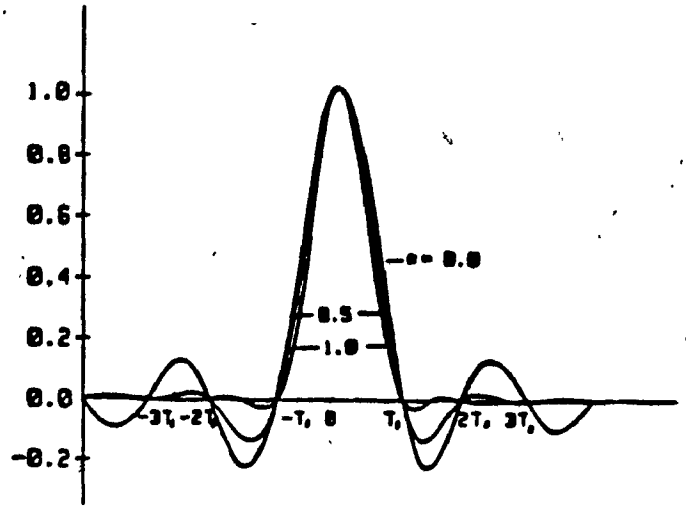

(a) Time Response

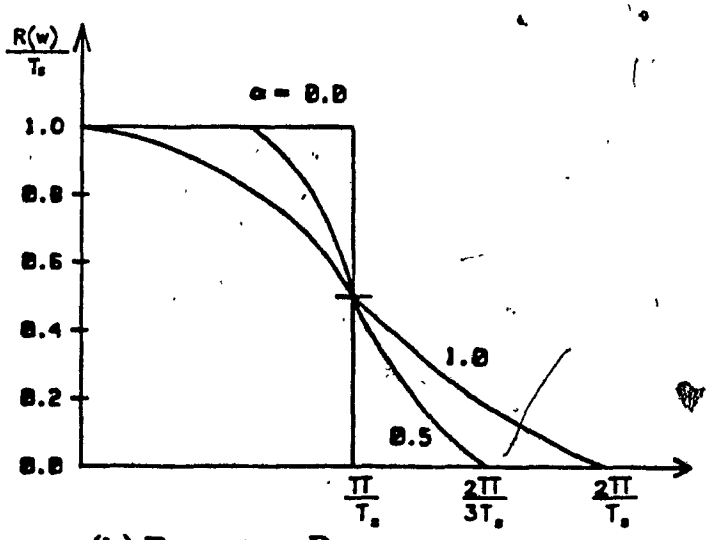

(b) Frequency Response

Figure 3.5 Raised-cosine pulse shaping.

3.1.4 Performance Analysis

In an AWGN and ISI free transmission with Nyquist filter partition, the sampled signal components $i(kT_s)$ and $q(kT_s)$ are represented by the signal constellation diagram as shown in Figure 3.3. The M-ary QAM is formed by two independent $\sqrt{M}$ -PAM components on two orthogonal axes. The probability of symbol error of M-ary QAM can be derived from that of $\sqrt{M}$ -PAM [15].

The averaged power of each $\sqrt{M}$ -ary PAM component is

$$P_{av} = \frac{\overline{a_i^2}}{2\pi T_s} \int_{-\infty}^{+\infty} R(w)dw \tag{3.17}$$

Since

$$\int_{-\infty}^{+\infty} |G_T(\omega,\alpha)|^2 d\omega = \int_{-\infty}^{+\infty} R(\omega,\alpha)d\omega = 2\pi \tag{3.18}$$

The average power becomes

$$P_{av} = \frac{\overline{a_i^2}}{T_s} \tag{3.19}$$

which is independent of the roll-off parameter α.

There are $\sqrt{M}$ equally likely amplitude values placed at the levels $\pm 1, \pm 3, \ldots\ldots, \pm(\sqrt{M}-1)$, hence

$$\overline{a_i^2} = \frac{2}{\sqrt{M}} \sum_{i=1}^{\sqrt{M}/2} [d(2i-1)]^2 = \frac{d^2}{3(M-1)} \tag{3.20}$$

where $\sqrt{M}$ is an even integer.

The average power of each $\sqrt{M}$ -ary PAM component is

$$P_{av} = \frac{d^2}{T_s} \frac{M-1}{3} \tag{3.21}$$

The transmitted power of M-ary QAM signal is

$$P_T = 2P_{av} = \frac{2d^2}{T_s} \frac{M-1}{3} \tag{3.22}$$

The symbol energy of M-ary QAM is

$$E_s = P_T T_s = \frac{2d(M-1)}{3} \tag{3.23}$$

For an AWGN channel, the sampled noise value $n_I'(iT_s)$ or $n_Q'(iT_s)$ is also a Gaussian random variable with variance

$$\sigma^2 = \frac{N_0/2}{2\pi} \int_{-\infty}^{+\infty} R(w)dw = \frac{N_0}{2} \tag{3.24}$$

For an $\sqrt{M}$ -PAM signal, there are $\sqrt{M}$ signal points : two outer points 0 and $(\sqrt{M}-1)$, and 1,.....,$(\sqrt{M}-2)$ inner points. The outer points can only be in error in one direction, while the inner points can be in error in two directions. The signal points representation is shown in Figure 3.6.

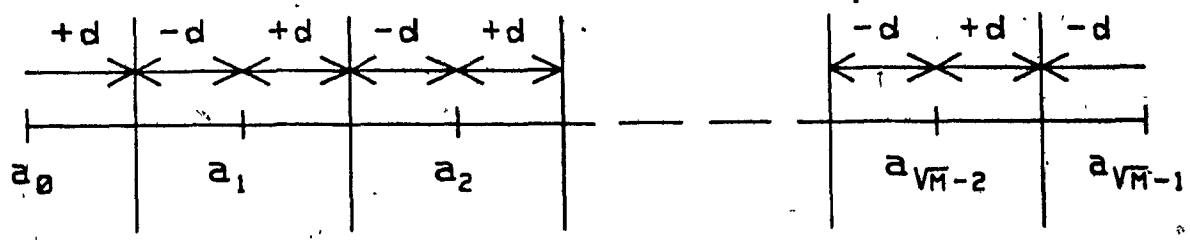

Figure 3.6 Signal points of $\sqrt{M}$ -ary PAM.

For $i=1;2,.....,(\sqrt{M}-2)$ the probability of correct detection of each signal point is given by

$$P_R\{c/a_i\} = \int_{-d}^{+d} \frac{1}{\sqrt{2\pi\sigma^2}} e^{-\frac{x^2}{2\sigma^2}} dx \qquad (3.25)$$

It can be put into a more convenient form by letting $y = \frac{x}{\sigma\sqrt{2}}$. Doing this, and utilizing the symmetry property of Gaussian function, equation (3.25) becomes

$$P_R\{c/a_i\} = \frac{2}{\sqrt{\pi}} \int_0^{\frac{d}{\sigma\sqrt{2}}} e^{-y^2} dy \qquad (3.26)$$

Therefore, the probability error for each signal point is

$$P_R\{error/a_i\} = 1 - \frac{2}{\sqrt{\pi}} \int_0^{\frac{d}{\sigma\sqrt{2}}} e^{-y^2} dy$$

$$= 1 - \left[1 - \frac{2}{\sqrt{\pi}} \int_{\frac{d}{\sigma\sqrt{2}}}^{+\infty} e^{-y^2} dy \right]$$

$$= \frac{2}{\sqrt{\pi}} \int_{\frac{d}{\sigma\sqrt{2}}}^{+\infty} e^{-y^2} dy$$

$$= erfc\left(\frac{d}{\sigma\sqrt{2}} \right) \tag{3.27}$$

For $i = 0, (\sqrt{M} - 1)$, these two outer signal points can only be in error in one direction each, and according to equation (3.27), hence, the probability of error is

$$P_R\{error / a_{\sqrt{M}-1}\} = P_R\{error / a_0\} = \frac{1}{2} erfc\left\{ \frac{d}{\sigma\sqrt{2}} \right\} \tag{3.28}$$

The probability of error averaged over all transmitted signals is then

$$P_{\sqrt{M}} = \left[\frac{(\sqrt{M} - 2)}{\sqrt{M}} + \frac{1}{\sqrt{M}} \right] erfc\left(\frac{d}{\sigma\sqrt{2}} \right)$$

$$= \left(1 - \frac{1}{\sqrt{M}} \right) erfc\left(\frac{d}{\sigma\sqrt{2}} \right) \tag{3.29}$$

The probability of symbol error of M-ary QAM signal is given by [15]

$$P_M = 1 - (1 - P_{\sqrt{M}})^2$$

$$= 2P_{\sqrt{M}} - P^2_{\sqrt{M}}$$

$$= 2\left[1 - \frac{1}{\sqrt{M}}\right]\left[\frac{d}{\sigma\sqrt{2}}\right] - \left[1 - \frac{1}{\sqrt{M}}\right]^2 erfc^2\left[\frac{d}{\sigma\sqrt{2}}\right]$$

$$\approx 2\left[1 - \frac{1}{\sqrt{M}}\right] erfc\left[\frac{d}{\sigma\sqrt{2}}\right] \qquad (3.30)$$

Replacing $d = \sqrt{3E_s/2(M-1)}$ and $\sigma^2 = N_0/2$ into equation (3.30), the probability of symbol error for M-ary QAM in an AWGN channel with Nyquist filter partitioning is

$$P_M = 2\left[1 - \frac{1}{\sqrt{M}}\right] erfc\left[\sqrt{\frac{3}{2(M-1)}\frac{E_s}{N_0}}\right] \qquad (3.31)$$

3.2 Performance analysis of M-ary QAM in an MPF channel

To study the performance of M-ary QAM in an MPF channel, a two-path fading model simulator is used (Figure 3.7).

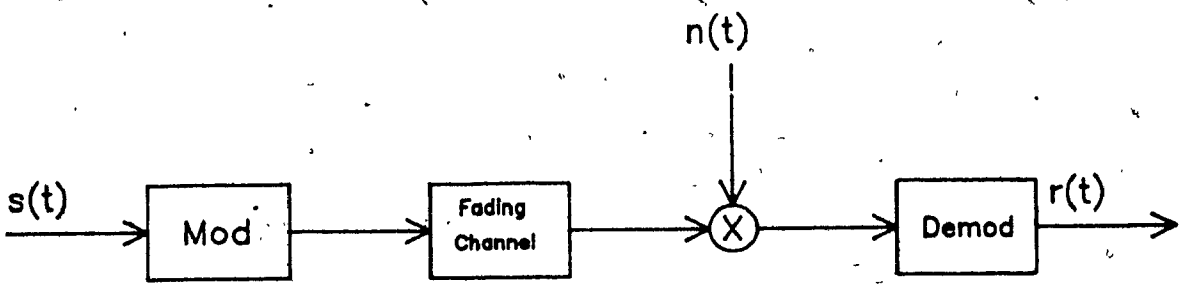

Figure 3.7 Block diagram of an MPF channel.

The received signal in a two-path MPF channel model is

$$r_{MPF}(t) = s(t) + \beta s(t-\tau) + n(t) \tag{3.32}$$

where n(t) is the AWGN represented by equation (3.5).

Substituting equations (3.3) and (3.5) into equation (3.32), the received signal becomes

$$r_{MPF}(t) = [I(t) + \beta I(t-\tau)\cos\omega_c\tau - \beta Q(t-\tau)\sin\omega_c\tau + n_I(t)]\cos\omega_c t$$
$$+ [Q(t) + \beta Q(t-\tau)\cos\omega_c\tau + \beta Q(t-\tau)\sin\omega_c\tau + n_Q(t)]\sin\omega_c t \tag{3.33}$$

After demodulation, low-pass filtering and scaling, the in-phase and quadrature baseband components become

$$i_{MPF}(t) = [I(t) + \beta I(t-\tau)\cos\omega_c\tau - \beta Q(t-\tau)\sin\omega_c\tau] * g_R(t) + n_I'(t) \tag{3.34}$$

and

$$q_{MPF}(t) = [Q(t) + \beta Q(t-\tau)\cos\omega_c\tau - \beta I(t-\tau)\sin\omega_c\tau] * g_R(t) + n_Q'(t) \tag{3.35}$$

where

$$n_I'(t) = n_I(t) * g_R(t) \tag{3.36}$$

$$n_Q'(t) = n_Q(t) * g_R(t) \tag{3.37}$$

For $\tau \ll T_s$ where T_s is the symbol interval,

$$i(t-\tau) \approx i(t)$$

$$q(t-\tau) \approx q(t)$$

Therefore equations (3.34) and (3.35) become

$$i(t) \approx I(t) + \beta I(t)\cos\omega_c \tau - \beta Q(t)\sin\omega_c \tau \tag{3.38}$$

and

$$q(t) \approx Q(t) + \beta Q(t)\cos\omega_c \tau + \beta Q(t)\sin\omega_c \tau \tag{3.39}$$

Equations (3.38) and (3.39) can be written as

$$i_{MPF}(t) = I'(t)[1 + \Delta_I] + n_I'(t) \tag{3.40}$$

and

$$q_{MPF}(t) = Q'(t)[1 + \Delta_Q] + n_Q'(t) \tag{3.41}$$

where

$$\Delta_I = X_I\sqrt{1 + \Psi_I^2} = X_I B_I \tag{3.42}$$

$$\Delta_Q = X_Q\sqrt{1 + \Psi_Q^2} = X_Q B_Q \tag{3.43}$$

$$X_I = \beta\cos[\omega_c \tau + \tan^{-1}(\Psi_I)] \tag{3.44}$$

$$X_Q = \beta\cos[\omega_c \tau + \tan^{-1}(\Psi_Q)] \tag{3.45}$$

$$\Psi_I(t) = \frac{Q'(t)}{I'(t)} \tag{3.46}$$

$$\Psi_Q(t) = \frac{I'(t)}{Q'(t)} \tag{3.47}$$

It is noted that $I'(t)$ and $Q'(t)$ are the noise free in-phase and quadrature baseband components in the non-MPF case as defined by equations (3.8) and (3.9).

The signals $i_{MPF}(t)$ and $q_{MPF}(t)$ are sampled at every iT_s for detection. The sampled noise components $n_I'(t)$, $n_Q'(t)$ are Gaussian random variables with variance of $N_0/2$ as given by equation (3.24). The sampled noise-free component, $I'(iT_s)$ or $Q'(iT_s)$, has one of $\sqrt{M}$ possible values as defined by equations (3.8) and (3.9). Therefore $\sqrt{1+\Psi_I^2(iT_s)}$ and $\sqrt{1+\Psi_Q^2(iT_s)}$, in equations (3.45) and (3.46) respectively, are independent discrete random variables with identical probability

$$P[B] \in \{ P_i = P[B_i], \text{ all possible } i \} \tag{3.48}$$

X_I and X_Q are independent and identical random variables with probability density function $f_X(x)$ representing MPF fading.

Statistical characteristics of random variables of B and x will be discussed in sections 4.1 and 4.2.

In general, the probability of symbol error of M-ary QAM in an MPF channel can be computed from that of the $\sqrt{M}$-ary PAM as discussed in section 3.1.4.

$$P_{M,MPF} = 1 - (1 - P_{\sqrt{M},MPF})^2$$

$$\approx 2P_{\sqrt{M},MPF} \tag{3.50}$$

where $P_{\sqrt{M},MPF}$ is the probability of symbol error of $\sqrt{M}$-PAM in an MPF channel, and is derived as follows.

Consider the sampled value of $i_{MPF}(iT_s)$ of equation (3.40), it is

$$i_{MPF}(iT_s) = [1 + \Delta_I]I'(iT_s) + n_I'(iT_s) \tag{3.51}$$

As mentioned earlier, $I'(iT_s)$ has the same value as a_i, where a_i is the transmitted symbol. The noise-free component of $i_{MPF}(iT_s)$ is $(1 + \Delta_I)a_i$ for a given value of Δ_I as shown in Figure 3.8.

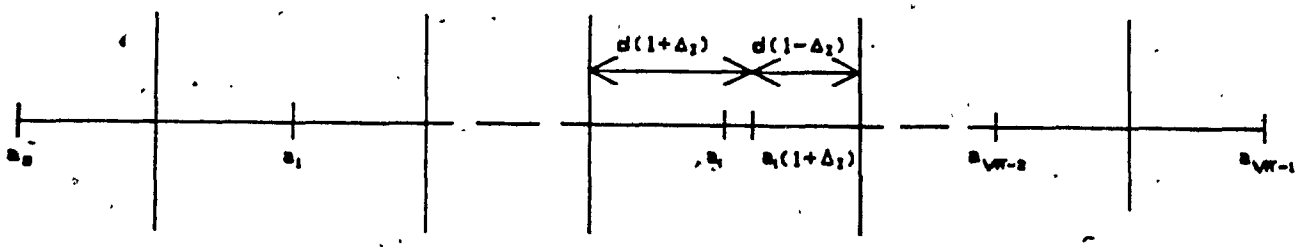

Figure 3.8 Signal diagram of $\sqrt{M}$ PAM in an MPF channel.

For $i = 1,2,.....,(\sqrt{M}-2)$, the conditional probability of the correct detection is

$$P[c/a_i, \Delta_I] = P[-d(1+\Delta_I) \leq n_I'(iT_s) \leq +d(1-\Delta_I)]$$

$$= \int_{+d(1-\Delta_I)}^{-d(1+\Delta_I)} \frac{1}{\sqrt{\pi N_0}} e^{-\frac{x^2}{N_0}} dx$$

$$= 1 - \frac{1}{2}\left[erfc\left(\frac{d(1-\Delta_I)}{\sqrt{N_0}}\right) + erfc\left(\frac{d(1+\Delta_I)}{\sqrt{N_0}}\right)\right] \quad (3.52)$$

For $i = 0, (\sqrt{M}-1)$

$$P[c/a_{0,}\Delta_I] = P[-\infty < n_I'(iT_s) \leq d(1-\Delta_I)]$$

$$= 1 - erfc\left(\frac{d(1-\Delta_I)}{\sqrt{N_0}}\right) \quad (3.53)$$

$$P[c/a_{\sqrt{M}-1},\Delta_I] = P[+\infty > n_I'(iT_s) \geq -d(1+\Delta_I)]$$

$$= 1 - erfc\left(\frac{d(1+\Delta_I)}{\sqrt{N_0}}\right) \quad (3.54)$$

The conditional probability of symbol error given a_i is

$$P[error/a_i] = \overline{P[error/a_i,\Delta_I]} = \sum_{all\ i} P[B_i] \int_{-\infty}^{+\infty} P[error/a_i,\Delta_I] f_z(x)dx$$

$$= \begin{cases} P(1-\Delta_I) & i = 0 \\ \frac{1}{2}[P(1-\Delta_I) + P(1+\Delta_I)] & i = 1,\ldots,(\sqrt{M}-2) \\ P(1+\Delta_I) & i = (\sqrt{M}-1) \end{cases} \quad (3.55)$$

where

$$P(1-\Delta_I) = \sum_{all\ i} P[B_i] \int_{-\infty}^{+\infty} erfc\left(\frac{d(1-\Delta_I)}{\sqrt{N_0}}\right) f_X(x)dx \tag{3.56}$$

$$P(1+\Delta_I) = \sum_{all\ i} P[B_i] \int_{-\infty}^{+\infty} erfc\left(\frac{d(1+\Delta_I)}{\sqrt{N_0}}\right) f_X(x)dx \tag{3.57}$$

Since Δ_I having values symmetric about zero

$$P(1-\Delta_I) = P(1+\Delta_I) \tag{3.58}$$

Therefore, the probability of symbol error of $\sqrt{M}$ -ary PAM signal in an MPF channel is

$$P_{\sqrt{M},MPF} = \sum_{i=0}^{\sqrt{M}-1} P[a_i]P[error/a_i]$$

$$= \left(1-\frac{1}{\sqrt{M}}\right) P(1+\Delta_I) \tag{3.59}$$

and the probability of symbol errors of M-ary QAM in an MPF channel is

$$P_{M,MPF} = 2\left(1-\frac{1}{\sqrt{M}}\right) P(1+\Delta_I) \tag{3.60}$$

with

$$P(1+\Delta_I) = \sum_{all\ i} P[B_i] \int_{-\infty}^{+\infty} erfc\left(\frac{d(1+\Delta_I)}{\sqrt{N_0}}\right) f_X(x)dx \tag{3.61}$$

$$d = \sqrt{\frac{3}{2(M-1)} E_s}$$

$$P(1+\Delta_I) = \sum_{all\ i} P[B_i] \int_{-\infty}^{+\infty} erfc\left[(1+B_i x)\sqrt{\frac{3}{2(M-1)}\frac{E_s}{N_0}}\right] f_X(x)dx \quad (3.62)$$

Hence, the final expression for the probability of symbol error is

$$P_{M,MPF} = 2\left(1 - \frac{1}{\sqrt{M}}\right) \sum_{all\ i} P[B_i] \int_{-\infty}^{+\infty} erfc\left[(1+B_i x)\sqrt{\frac{3}{2(M-1)}\frac{E_s}{N_0}}\right] f_X(x)dx$$

$$= 2\left(1-\frac{1}{\sqrt{M}}\right) \sum_{all\ i} P[B_i] \int_{-\infty}^{+\infty} erfc\left[(1+B_i x)\sqrt{\gamma_s}\right] f_X(x)dx \quad (3.63)$$

where

$$\sqrt{\gamma_s} = \sqrt{\frac{3}{2(M-1)}\frac{E_s}{N_0}}$$

CHAPTER IV

PERFORMANCE OF M-ARY QAM SYSTEMS IN AN MPF CHANNEL

PART II : EXPLICIT EXPRESSIONS

4.1 Statistical Characteristics of B_i

In an M-ary QAM system, the amplitude $\{a_i\}$, and $\{b_i\}$ are identically distributed random variables which have the following values and probabilities.

16-QAM

$i(iT_s) = \pm 1, \pm 3$ *each with prob* $\frac{1}{4}$

$q(iT_s) = \pm 1, \pm 3$ *each with prob* $\frac{1}{4}$

64-QAM

$i(iT_s) = \pm 1, \pm 3, \pm 5, \pm 7$ *each with prob* $\frac{1}{8}$

$q(iT_s) = \pm 1, \pm 3, \pm 5, \pm 7$ *each with prob* $\frac{1}{8}$

256-QAM

$i(iT_s) = \pm 1, \pm 3, \pm 5, \pm 7, \pm 9, \pm 11, \pm 13, \pm 15$ each with prob $\frac{1}{16}$

$q(iT_s) = \pm 1, \pm 3, \pm 5, \pm 7, \pm 9, \pm 11, \pm 13, \pm 15$ each with prob $\frac{1}{16}$

The values of B_i and the corresponding probabilities $P\{B_i\}$ for 16, 64 and 256-QAM are given in Tables I, II and III. In the above amplitude values of $\{a_i\}$ and $\{b_i\}$'s, d is normalized to unity without loss of physical insight.

Table 4.1

Probability B_i of 16-QAM

B_i	$P\{B_i\}$
3	1/4
1	1/2
1/3	1/4

Table 4.2

Probability B_i of 64-QAM

B_i	$P\{B_i\}$
7	1/16
3	1/16
7/3	1/16
5/3	1/16
7/5	1/16
1	1/4
5/7	1/16
3/5	1/16
3/7	1/16
1/3	1/16
1/5	1/16
1/7	1/16

Table 4.3

Probability B_i of 256-QAM

B_i	$P\{B_i\}$
1/15	1/64
1/13	1/64
1/11	1/64
1/9	1/64
1/7	1/64
1/5	1/32
3/13	1/64
1/3	3/64
5/3	1/64
3/7	1/64
5/11	1/64
7/15	1/64
7/13	1/64
5/9	1/64
9/5	1/32
7/11	1/64
9/13	1/64
5/7	1/64
11/15	1/64
7/9	1/32
9/11	1/64
11/13	1/64
13/15	1/64
1	1/8

B_i	$P\{B_i\}$
15/13	1/64
13/11	1/64
11/9	1/64
9/7	1/64
15/11	1/64
7/5	1/64
13/9	1/64
11/7	1/64
5/3	1/32
9/5	1/64
13/7	1/64
15/7	1/64
11/5	1/64
7/3	1/64
13/5	1/64
3	3/64
11/3	1/64
13/5	1/64
5	1/32
7	1/64
9	1/64
11	1/64
13	1/64
15	1/64

4.2 Statistical Characteristics of x

Equations (3.44) can be written as

$$x = \beta\cos[\omega_c \tau + \tan^{-1}(\Psi)] \tag{4.1}$$

The effect of MPF is determined by the parameters β and τ. Both β and τ are assumed to be random variables. To study the effect of MPF, it is essential to find the statistical property of rv x.

4.2.1 Probability Density Function of The Cosine Function

Let us define an rv z as

$$z = \cos[\omega_c \tau + \tan^{-1}(\Psi)] = \cos\theta \tag{4.2}$$

where θ is an rv, ω_c and $\tan^{-1}(\Psi)$ are constants. The rv θ represents the random phase of the cosine function.

The PDF of z is determined by the transformation method as given by Papoulis [30].

$$f_Z(z) = \sum_j \frac{f_\Theta(\theta_n)}{|f'(\theta_n)|} = \frac{1}{\sqrt{1-z^2}} \sum_j f_\Theta(\theta_n) \quad |z| < 1 \tag{4.3}$$

for any equation $z = f(\theta)$.

where θ_n, $n = 1,2,....,n$ are the real roots of the equation $z = f(\theta)$ and $f'(\theta)$ is the derivation of $f(\theta)$.

In each interval of 2π, $\sum_j f_\Theta(\theta_n)$ has two terms. If θ is uniform on an interval of 2π, then the two solutions for z are inside the applicable interval. The function $f_\Theta(\theta_n)$ is equal to $1/2\pi$ for each of these solutions and vanished outside the interval. Adding these two terms and substituting into equation (4.3), the solution of $f_Z(z)$ becomes

$$f_Z(z) = \frac{1}{\pi\sqrt{1-z^2}} \qquad |z| < 1 \qquad (4.4)$$

4.4.2 Probability Density Function of β

Greenstein and Prabhu have suggested an exponential form for the PDF of β [12].

$$f_\beta(\beta) = \frac{\lambda}{1-e^{\lambda}}\exp(-\lambda(1-\beta)) \qquad 0 \leq \beta \leq 1 \qquad (4.5)$$

This expression is intuitively attractive and easy to analyze. However, it is preferrable to vary λ so that different fading conditions can be modeled. In order to do so, the following convention is suggested.

If the sign of λ is negative, fading conditions are more severe; if positive, fading conditions are less severe.

The parameter λ in equation (4.5), therefore, experiences a sign reversal. The suitable density function for β is then :

$$f_{\beta}(\beta) = \frac{\lambda}{e^{\lambda} - 1} \exp(\lambda(1 - \beta)) \tag{4.6}$$

where $0 \leq \beta \leq 1$ $\quad -\infty \leq \lambda \leq \infty$

This validity of this PDF to characterize different fading conditions is now investigated.

(a) At Positive Extreme Value $\lambda \rightarrow +\infty$

$$\lim_{\beta \rightarrow +\infty} f_{\beta}(\beta) = \delta(\beta) \tag{4.7}$$

In practice, this means that there is no reflection and thus no MPF.

(b) At Negative Extreme Value $\lambda \rightarrow -\infty$

$$\lim_{\lambda \rightarrow -\infty} f_{\beta}(\beta) = \delta(1-\beta) \tag{4.8}$$

In practice, this means that the reflection is always as large as the direct signal. It is the worst MPF condition.

(c) At Middle Value $\lambda = 0$

$$\lim_{\lambda \to 0} f_{\beta}(\beta) = 1 \qquad 0 \leq \beta \leq 1 \tag{4.9}$$

The relative amplitude of the reflection can assume any value with equal probability.

It is concluded that expression $f_{\beta}(\beta)$ in (4.6) represents a family of PDF 's which covers all the range of MPF conditions.

4.2.3 Probability Density Function of x

It has been shown that feasible solutions are obtainable for the PDF of β and the cosine function, respectively. It is essential now to find the PDF of x which combines the effect of β and the cosine function. Again β and τ are assumed to be statistically independent. Hence, for a uniform θ, it can be shown that the PDF of x is given by [30]

$$f_X(x) = \frac{1}{\pi} \int_{-\infty}^{-|x|} \frac{f_{\beta}(y)}{\sqrt{y^2 - x^2}} dy + \frac{1}{\pi} \int_{|x|}^{+\infty} \frac{f_{\beta}(y)}{\sqrt{y^2 - x^2}} dy \tag{4.10}$$

where y is a dummy variable.

But the PDF of β is defined in the $0 \leq \beta \leq 1$ interval only. Hence equation (4.10) becomes

$$f_X(x) = \frac{K(\lambda)}{\pi} \int_{|x|}^{1} \frac{e^{-\lambda y}}{\sqrt{y^2 - x^2}} dy \qquad |x| < 1 \qquad (4.11)$$

where

$$K(\lambda) = \frac{\lambda e^{\lambda}}{e^{\lambda} - 1} \qquad \text{and} \qquad -\infty \leq \lambda \leq \infty$$

A few important observations are listed in the following :

(1) when $\lambda \rightarrow +\infty$, then $\beta = 0$ with probability equal one. There is no reflection.

(2) when $\lambda \rightarrow -\infty$, then $\beta = 1$ with probability equal one. The PDF becomes

$$f_X(x) = \frac{1}{\sqrt{1 - x^2}} \qquad |x| < 1 \qquad (4.12)$$

(3) when $\lambda = 0$, the PDF becomes

$$f_X(x) = \frac{1}{\pi} [ln\,(1 + \sqrt{1 - x^2} - ln\,|x|] \qquad (4.13)$$

(4) For other values of λ, the PDF function remains symmetric at $x = 0$ and follows approximately an exponentially form.

Equation (4.13) at the middle value $\lambda = 0$ is shown in Figure 4.1. It has approximate an exponential form, and it may be relatively well approximated by a linear function.

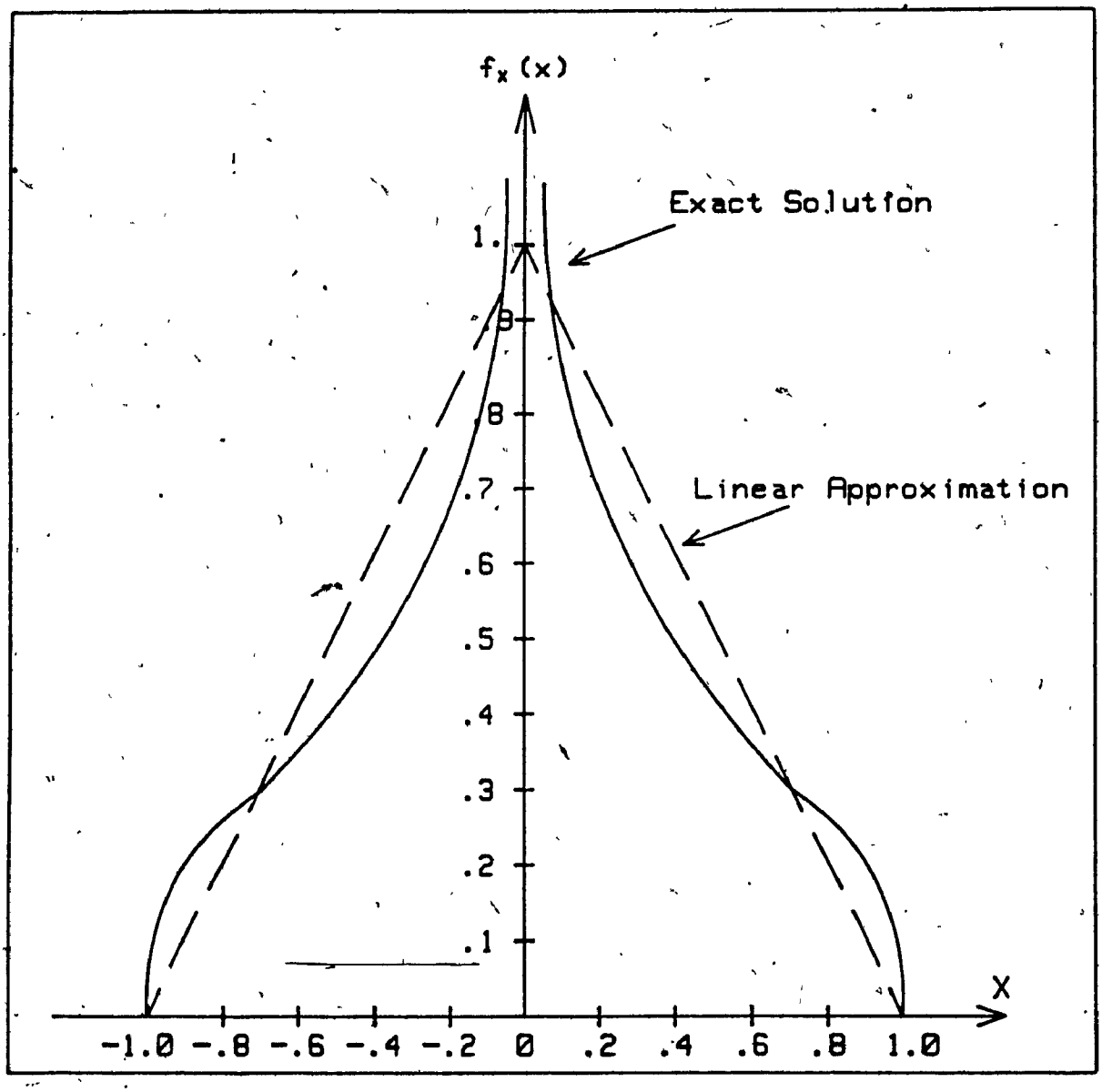

Figure 4.1 The PDF of x at $\lambda = 0$

4.2.4 Direct Postulation of The Probability Function of x

As the fading conditions, represented by λ, change, the integration in (4.6) needs to be re-evaluated. Furthermore, for certain values of λ, the exact solutions do not exist. Therefore, the analysis of system performance would be very complicated, inconvenient and impractical.

To avoid the above mention difficulties, Brana & Le-Ngoc [5,6] have postulated a compatible form for the PDF instead of finding the exact solution. They analyzed the performance behavior of equation (4.6) at certain specific values, and then postulated a direct compatible solution which has approximately the same behavior as the exact solution.

According to the analysis in section 4.2.3, the PDF $f_X(x)$ must satisfy the following requirements.

(1) The PDF of x will be symmetrical about $x = 0$ and follow approximately an exponential form.

(2) The probability density of $x = -1$ and $x = 1$ should be zero. This property can be deduced from the property of the cosine function. The density increases when it approaches these values, but it never actually reaches the values.

(3) From the probability theory, the PDF must satisfy

$$f_X(x) \geq 0 \qquad -1 \leq x \leq 1 \tag{4.14}$$

$$\int_{-1}^{+1} f_X(x)dx = 1 \tag{4.15}$$

Based on the above assumptions, these properties cannot be satisfied by a purely exponential function. The best approximation is using a function with an exponential part plus a negative constant part. Therefore, the postulated solution is

$$f_X(x) = \frac{\lambda\, e^{\lambda}}{2(\, e^{\lambda} - \lambda - 1\,)} \exp(-\lambda \mid x \mid) - \frac{\lambda}{2(\, e^{\lambda} - \lambda - 1\,)} \tag{4.16}$$

where $-1 \leq x \leq 1$ and $-\infty < \lambda < +\infty$

Such a solution follows approximately the behavior of equation (4.11). It reduces mathematical complexity but keeps the flexibility to model different fading conditions by simply varying the parameter λ.

For a finite negative λ, equation (4.15) is exponential and decreases rather slowly towards the extreme values ($x = 1$ and $x = -1$). For a finite positive λ, the function is also exponential but decreases rather rapidly towards the extremes. The behavior of equation (4.16) will now be investigated in detail for the three specific values of λ : $-\infty$, $+\infty$, and 0.

(a) Positive extreme $\lambda \to +\infty$

$$\lim_{\lambda \to \infty} f_X(x) = \delta(x) \tag{4.17}$$

Hence, when $\lambda \rightarrow +\infty$ (the best channel conditions) the probability is 1 at $x = 0$ and vanishes elsewhere. It means that no MPF exists.

(b) Negative extreme $\lambda \rightarrow -\infty$

$$\lim_{\lambda \rightarrow -\infty} f_X(X) = \frac{1}{2} \tag{4.18}$$

Fading conditions given by this case are quite severe and will drastically degrade the performance of the transmission system.

(c) Middle value $\lambda = 0$

$$\lim_{\lambda \rightarrow 0} = 1 - |x| \qquad -1 \leq x \leq 1 \tag{4.19}$$

The PDF reduces to a linear function. This result is consistent with the behavior observed by applying the method of the transformation of rv in section 4.2.1.

4.3 Expressions for Probability of Symbol Error

In this section, the probability of symbol error for M-ary QAM signals are developed, based on the statistical model formulated in sections 4.1 and 4.2. Their performance under various fading conditions are evaluated and illustrated.

4.3.1 Integral Equation

The final expression for the probability of symbol error, equation (3.64), is repeated here for convenience.

$$P_{M,MPF} = 2\left(1-\frac{1}{\sqrt{M}}\right)\sum_{all\ i} P[B_i]\int_{-\infty}^{+\infty} erfc\left[(1+B_i x)\sqrt{\gamma_s}\right] f_X(x)dx \quad (4.20)$$

where $f_X(x)$ is the PDF of x , and $|x| \leq 1$ from equation (4.16).

Hence, the average probability of symbol error can be expressed as

$$P_{M,MPF} = 2\left(1-\frac{1}{\sqrt{M}}\right)\sum_{all\ i} P[B_i]\int_{-1}^{+1} erfc\left[(1+B_i x)\sqrt{\gamma_s}\right] f_X(x)\ dx$$

$$= 2\left(1-\frac{1}{\sqrt{M}}\right)\sum_{all\ i} P[B_i]T_i \quad (4.21)$$

$$T_i = \int_{-1}^{+1} erfc\left[(1+B_i x)\sqrt{\gamma_s}\right] f_X(x)dx \quad (4.22)$$

and

$$erfc(x) = \frac{2}{\sqrt{\pi}}\int_x^{\infty} e^{-t^2}dt$$

$$= 1 - erf(x)$$

$$= 1 + erf(-x) \quad (4.23)$$

At the interval $-1 \leq x \leq -\frac{1}{B_i}$, the argument of the error complementary function becomes negative. In order to compute T_i and the probability of symbol error, equation (4.22) has to divide into two parts : the first part deals with the negative argument, and the second part with the positive argument.

As a result, equation (4.22) can be expressed as

$$T_i = \int_{-1}^{+1} f_X(x)dx + \int_{-1}^{-\frac{1}{B_i}} erf\{-(1+B_i x)\sqrt{\gamma_s}\} f_X(x)dx$$

$$- \int_{-\frac{1}{B_i}}^{+1} erf\{(1+B_i x)\sqrt{\gamma_s}\} f_X(x)dx$$

$$= 1 + \int_{-1}^{-\frac{1}{B_i}} erf\{-(1+B_i x)\sqrt{\gamma_s}\} f_X(x)dx$$

$$- \int_{-\frac{1}{B_i}}^{+1} erf\{(1+B_i x)\sqrt{\gamma_s}\} f_X(x)dx \qquad (4.24)$$

4.3.2 Probability of Symbol Error at $\lambda \to -\infty$

From equation (4.18), the PDF $f_X(x)$ at negative values λ approaching $-\infty$ equals 1/2 . Substituting this value into equation (4.24), T_i then becomes

$$T_i = \left[1 + \int_{-1}^{-\frac{1}{B_i}} \frac{1}{2} erf\ \{(1+B_i x)\sqrt{\gamma_s}\}dx - \int_{-\frac{1}{B_i}}^{+1} \frac{1}{2} erf\ \{(1+B_i x)\sqrt{\gamma_s}\}dx \right]$$

$$= \left[1 + I_1 + I_2\right] \tag{4.25}$$

To evaluate equation (4.25), the following equation is used [31].

$$\int erf\ \{x\}dx = x erf\ \{x\} + \frac{1}{\sqrt{\pi}} e^{-x^2} \tag{4.26}$$

Equation (4.26) can be expressed as

$$\int_{L1}^{L2} erf\ \{ax\}dx = \frac{1}{a}\left[x erf\ \{x\} + \frac{1}{\sqrt{\pi}} e^{-x^2}\right]_{aL_1}^{aL_2} \tag{4.27}$$

Expression I_1 of equation (4.25) is

$$I_1 = \int_{-1}^{-\frac{1}{B_i}} \frac{1}{2} erf\ \{-(1+B_i x)\sqrt{\gamma_s}\}dx \tag{4.28}$$

Let $\quad y = -(1+B_i x) \qquad dy = -B_i dx$

$$At \quad x = -\frac{1}{B_i} \qquad y = 0$$

$$x = -1 \qquad y = B_i - 1$$

After the substitution, I_1 becomes

$$I_1 = -\frac{1}{2B_i} \int_{(B_i-1)}^{0} erf\ \{y\sqrt{\gamma_s}\}\, dy \tag{4.29}$$

By applying equation (4.27), I_1 becomes

$$I_1 = -\frac{1}{2B_i\sqrt{\gamma_s}} \left[y\, erf\ \{y\} + \frac{1}{\sqrt{\pi}} e^{-y^2} \right]_{(B_i-1)\sqrt{\gamma_s}}^{0}$$

$$= \frac{(B_i-1)}{2B_i} erf\ \{(B_i-1)\sqrt{\gamma_s}\} - \frac{1}{2B_i\sqrt{\gamma_s \pi}} \left[1 - e^{-(B_i-1)^2\gamma_s} \right] \tag{4.30}$$

Expression I_2 of equation (4.25) is

$$I_2 = -\frac{1}{2B_i} \int_{-\frac{1}{B_i}}^{+1} erf\ \{(1 + B_i x)\sqrt{\gamma_s}\}\, dy \tag{4.31}$$

$$Let \quad y = 1 + B_i x \qquad dy = B_i\, dx$$

$$At \quad x = 1 \qquad y = B_i + 1$$

$$x = -\frac{1}{B_i} \qquad y = 0$$

After substitution, expression I_2 becomes

$$I_2 = -\frac{1}{2B_i}\int_0^{B_i+1} erf\ \{y\sqrt{\gamma_s}\}dy \tag{4.32}$$

By applying equation (4.27) again, I_2 can be written as

$$I_2 = -\frac{1}{2B_i\sqrt{\gamma_s}}\left[y erf\ \{y\} + \frac{1}{\sqrt{\pi}}e^{-y^2}\right]_0^{(B_i+1)\sqrt{\gamma_s}}$$

$$= -\frac{(B_i+1)}{2B_i} erf\ \{(B_i+1)\sqrt{\gamma_s}\} + \frac{1}{2B_i\sqrt{\gamma_s\pi}}\left[1-e^{-(B_i+1)^2\gamma_s}\right] \tag{4.33}$$

Substituting equations (4.30) and (4.33) into (4.25), T_i becomes

$$T_i = \left[1 + I_1 + I_2\right]$$

$$= \left[1 + \frac{(B_i-1)}{2B_i} erf\ \{(B_i-1)\sqrt{\gamma_s}\} - \frac{(B_i+1)}{2B_i} erf\ \{(B_i+1)\sqrt{\gamma_s}\}\right]$$

$$+ \frac{1}{2B_i\sqrt{\gamma_s\pi}}\left[e^{-(B_i-1)^2\gamma_s} - e^{-(B_i+1)^2\gamma_s}\right] \tag{4.34}$$

From equation (4.21), the probability of symbol error is

$$P_{M,MPF} = 2\left(1-\frac{1}{\sqrt{M}}\right)\sum_{all\ i} P[B_i]\left[1 + \frac{(B_i-1)}{2B_i} erf\ \{(B_i-1)\sqrt{\gamma_s}\} - \frac{(B_i+1)}{2B_i} erf\ \{(B_i+1)\sqrt{\gamma_s}\}\right]$$

$$+ 2\left(1-\frac{1}{\sqrt{M}}\right)\sum_{all\ i} P[B_i]\frac{1}{2B_i\sqrt{\gamma_s\pi}}\left[e^{-(B_i-1)^2\gamma_s} - e^{-(B_i+1)^2\gamma_s}\right] \tag{4.35}$$

4.3.3 Probability of Symbol Error at $\lambda = 0$

From equation (4.19), the PDF $f_X(x)$ at the middle value $\lambda = 0$ equals $1-|x|$. Therefore, equation (4.22) becomes

$$T_i = \left[1 + \int_{-1}^{-\frac{1}{B_i}} erf\{-(1+B_i x)\sqrt{\gamma_s}\}(1-|x|)dx - \int_{-\frac{1}{B_i}}^{+1} erf\{(1+B_i x)\sqrt{\gamma_s}\}(1-|x|)dx \right]$$

$$= \left[1 + I_1 + I_2 \right] \tag{4.36}$$

To evaluate (4.36), the following equation is used [31]

$$\int x erf\{ax\}dx = \frac{x^2}{2} erf\{ax\} - \frac{1}{4a^2} erf\{ax\} + \frac{x}{2a\sqrt{\pi}} e^{-a^2x^2} \tag{4.37}$$

Expression I_1 of (4.36) is

$$I_1 = \int_{-1}^{-\frac{1}{B_i}} erf\{-(1+B_i x)\sqrt{\gamma_s}\}(1-|x|)dx$$

$$= \int_{-1}^{-\frac{1}{B_i}} erf\{-(1+B_i x)\sqrt{\gamma_s}\}dx + \int_{-1}^{-\frac{1}{B_i}} x erf\{-(1+B_i x)\sqrt{\gamma_s}\}dx \tag{4.38}$$

$$Let: \quad y = -(1+B_i x) \qquad dy = -B_i\, dx$$

$$At \quad x = -1 \qquad y = B_i - 1$$

$$x = -\frac{1}{B_i} \qquad y = 0$$

After substituting and rearranging I_1, the following expression is obtained

$$I_1 = \frac{1}{B_i^2}\int_{B_i-1}^{0} y\, erf\,\{y\sqrt{\gamma_s}\}dy - \frac{(B_i-1)}{B_i^2}\int_{B_i-1}^{0} erf\,\{y\sqrt{\gamma_s}\}dy \qquad (4.39)$$

Applying equation (4.37) to the first term of (4.39) and equation (4.27) to the second term, I_1 becomes

$$I_1 = \frac{1}{B_i^2}\left[\frac{y^2}{2} erf\,\{y\sqrt{\gamma_s}\} - \frac{1}{4\gamma_s} erf\,\{y\gamma_s\} + \frac{y}{2\sqrt{\gamma_s \pi}} e^{-\gamma_s y}\right]_{(B_i-1)}^{0}$$

$$- \frac{(B_i-1)}{B_i^2}\left[\frac{y}{\sqrt{\gamma_s}} erf\,\{y\} + \frac{1}{\sqrt{\gamma_s \pi}} e^{-y}\right]_{(B_i-1)\sqrt{\gamma_s}}^{0} \qquad (4.40)$$

Expanding equation (4.40), the final expression of I_1 is

$$I_1 = -\frac{(B_i-1)^2}{2B_i^2} erf\,\{(B_i-1)\sqrt{\gamma_s}\} + \frac{1}{4B_i^2\gamma_s} erf\,\{(B_i-1)\sqrt{\gamma_s}\} - \frac{(B_i-1)}{2B_i^2\sqrt{\gamma_s \pi}} e^{-(B_i-1)^2\gamma_s}$$

$$+ \frac{(B_i-1)^2}{B_i^2} erf\,\{(B_i-1)\sqrt{\gamma_s}\} + \frac{(B_i-1)}{B_i\sqrt{\gamma_s \pi}}\left[-e^{-(B_i-1)^2\gamma_s} - 1\right] \qquad (4.41)$$

Expression I_2 of equation (4.36) is

$$I_2 = -\int_{-\frac{1}{B_i}}^{+1} erf\ \{(1+B_i x)\sqrt{\gamma_s}\}(1-|x|)dx$$

$$= -\int_{-\frac{1}{B_i}}^{+1} erf\ \{(1+B_i x)\sqrt{\gamma_s}\}dx - \int_{-\frac{1}{B_i}}^{0} x erf\ \{(1+B_i x)\sqrt{\gamma_s}\}dx$$

$$+ \int_{0}^{+1} x erf\ \{(1+B_i x)\sqrt{\gamma_s}\}dx \qquad (4.42)$$

$$Let \quad y = 1+B_i x \qquad dy = B_i\, dx$$

$$At \quad x = -\frac{1}{B_i} \qquad y = 0$$

$$x = 1 \qquad y = 1+B_i$$

$$x = 0 \qquad y = 1$$

Substituting the above values to (4.42), I_2 becomes

$$I_2 = -\frac{1}{B_i}\int_{0}^{B_i+1} erf\ \{y\sqrt{\gamma_s}\}dy + \frac{1}{B_i^2}\int_{0}^{1} erf\ \{y\sqrt{\gamma_s}\}dy - \frac{1}{B_i^2}\int_{+1}^{B_i+1} erf\ \{y\sqrt{\gamma_s}\}dy$$

$$- \frac{1}{B_i}\int_{0}^{1} y erf\ \{y\sqrt{\gamma_s}\}dy + \frac{1}{B_i^2}\int_{1}^{B_i+1} y erf\ \{y\sqrt{\gamma_s}\}dy \qquad (4.43)$$

Applying equation (4.27) to the first three terms of equation (4.43), and equation (4.37) to the last two terms, expression I_2 becomes

$$I_2 = -\frac{1}{B_i\sqrt{\gamma_s}}\left[y\,erf\,\{y\} + \frac{1}{\sqrt{\pi}}e^{-y^2}\right]_0^{(B_i+1)\sqrt{\gamma_s}}$$

$$-\frac{1}{B_i^2}\left[\frac{y^2}{2}erf\,\{y\sqrt{\gamma_s}\} - \frac{1}{4\gamma_s}erf\,\{y\sqrt{\gamma_s}\} + \frac{y}{2\sqrt{\gamma_s\pi}}e^{-y^2\gamma_s}\right]_0^1$$

$$+\frac{1}{B_i^2\sqrt{\gamma_s}}\left[y\,erf\,\{y\} + \frac{1}{\sqrt{\pi}}e^{-y^2}\right]_0^{\sqrt{\gamma_s}}$$

$$+\frac{1}{B_i^2}\left[\frac{y^2}{2}erf\,\{y\sqrt{\gamma_s}\} - \frac{1}{4\gamma_s}erf\,\{y\sqrt{\gamma_s}\} + \frac{y}{2\sqrt{\pi\gamma_s}}e^{-y^2\gamma_s}\right]_1^{B_i+1}$$

$$-\frac{1}{B_i^2\sqrt{\gamma_s}}\left[y\,erf\,\{y\} + \frac{1}{\sqrt{\pi}}e^{-y^2}\right]_{\sqrt{\gamma_s}}^{(B_i+1)\sqrt{\gamma_s}} \qquad (4.44)$$

Expanding equation (4.44), the final expression of I_2 becomes

$$I_2 = -\frac{(B_i+1)}{B_i}erf\,\{(B_i+1)\sqrt{\gamma_s}\} - \frac{1}{B_i\sqrt{\gamma_s\pi}}e^{-(B_i+1)^2\gamma_s} + \frac{1}{B_i\sqrt{\gamma_s\pi}}$$

$$-\frac{1}{B_i^2}erf\,\{\sqrt{\gamma_s}\} + \frac{1}{4B_i^2\gamma_s}erf\,\{\sqrt{\gamma_s}\} - \frac{1}{2B_i^2\sqrt{\gamma_s\pi}}e^{-\gamma_s}$$

$$+\frac{1}{B_i^2}erf\,\{\sqrt{\gamma_s}\} + \frac{1}{B_i^2\sqrt{\gamma_s\pi}}e^{-\gamma_s} + \frac{1}{B_i^2\sqrt{\gamma_s\pi}}$$

$$+\frac{(B_i+1)^2}{2B_i^2}erf\,\{(B_i+1)\sqrt{\gamma_s}\} - \frac{1}{4B_i^2\gamma_s}erf\,\{(B_i+1)\sqrt{\gamma_s}\} + \frac{(B_i+1)}{2B_i^2\sqrt{\gamma_s\pi}}e^{-(B_i+1)^2\gamma_s}$$

$$-\frac{1}{2B_i^2}erf\,\{\sqrt{\gamma_s}\} + + \frac{1}{4\gamma_s B_i^2}erf\,\{\sqrt{\gamma_s}\} + \frac{1}{2B_i^2\sqrt{\gamma_s\pi}}e^{-\gamma_s}$$

$$- \frac{(B_i+1)^2}{B_i^2} erf\ \{(B_i+1)\sqrt{\gamma_s}\} - \frac{1}{B_i^2 \gamma_s \pi} e^{-(B_i+1)^2\gamma_s}$$

$$+ \frac{1}{B_i^2} erf\ \{\sqrt{\gamma_s}\} + \frac{1}{B_i^2\sqrt{\gamma_s \pi}} e^{-\gamma_s} \qquad (4.45)$$

Substituting equations (4.41) and (4.45) into equation (4.36), T_i becomes

$$T_i = \left[1 + I_1 + I_2\right]$$

$$= 1 + K_H erf\ \{\sqrt{\gamma_s}\} + K_I erf\ \{(B_i+1)\sqrt{\gamma_s}\} + K_J erf\ \{(B_i-1)\}\sqrt{\gamma_s}\}$$

$$+ K_K \exp(-\gamma_s) - K_L \exp(-(B_i+1)^2\gamma_s) + K_M \exp(-(B_i+1)^2\gamma_s) \qquad (4.46)$$

From equation (4.21), the probability of symbol error is

$$P_{M,MPF} = 2\left(1-\frac{1}{\sqrt{M}}\right)\sum_{all\ i} P[B_i]\left[1 + K_H erf\ \{\sqrt{\gamma_s}\} + K_I erf\ \{(B_i+1)\sqrt{\gamma_s}\}\right]$$

$$+ 2\left(1-\frac{1}{\sqrt{M}}\right)\sum_{all\ i} P[B_i]\left[1 + K_J erf\ \{(B_i-1)\}\sqrt{\gamma_s}\} + K_K \exp(-\gamma_s)\right]$$

$$- 2\left(1-\frac{1}{\sqrt{M}}\right)\sum_{all\ i} P[B_i]\left[K_L \exp(-(B_i+1)^2\gamma_s) - K_M \exp(-(B_i+1)^2\gamma_s)\right] \qquad (4.47)$$

where

$$K_H = \frac{1}{2} + \frac{1}{4\gamma_s}$$

$$K_J = \frac{(B_i-1)^2}{2B_i^2} + \frac{1}{4B_i^2\gamma_s}$$

$$K_I = -\left[\frac{(B_i+1)^2}{2B_i} + \frac{1}{4\gamma_s}\right]$$

$$K_K = \frac{1}{B_i^2\sqrt{\gamma_s \pi}}$$

$$K_L = \frac{(B_i+1)}{2B_i^2\sqrt{\gamma_s \pi}}$$

$$K_M = \frac{(B_i-1)}{2B_i^2\sqrt{\gamma_s \pi}}$$

4.3.4 Probability of Symbol Error for General Value of λ

Section 4.3.2 and 4.3.3 deal with special cases of PDF, the probability symbol error of both cases are evaluated at the specific values of λ. In this section, a general expression of probability of symbol error will be evaluated. In this case, λ is a variable representing different fading conditions.

Substituting equation (4.16) into equation (4.22), T_i becomes

$$T_i = \left[1 + \int_{-1}^{\frac{1}{B_i}} \{-(1+B_i x)\gamma_s\}(K_1 \exp(-\lambda \mid x \mid) - K_2)dx - \int_{-\frac{1}{B_i}}^{1} erf\ \{(1+B_i x)\sqrt{\gamma_s}\}(K_1 \exp(-\lambda \mid x \mid) - K_2)dx \right]$$

$$= \left[1 + I_1 + I_2\right] \qquad (4.48)$$

To evaluate equation (4.48), the following equation is used [31]

$$\int e^{ax} erf\ \{bx\}dx = \frac{1}{a}\left[e^{ax} erf\ \{bx\} - e^{\frac{a^2}{4b^2}} erf\left\{ bx - \frac{a}{2b} \right\} \right] \qquad (4.49)$$

Expression I_1 of equation (4.48) is

$$I_1 = \int_{-1}^{\frac{1}{B_i}} erf\ \{-(1+B_i x)\sqrt{\gamma_s}\}(K_1 e^{-\lambda \mid X \mid} - K_2)dx$$

$$= \int_{-1}^{-\frac{1}{B_i}} K_1 e^{\lambda x} erf\ \{-(1+B_i x)\sqrt{\gamma_e}\}dx - \int_{-1}^{-\frac{1}{B_i}} K_2 erf\ \{-(1+B_i x)\sqrt{\gamma_e}\}dx \qquad (4.50)$$

$$Let \quad y = -(1+B_i x) \qquad dy = B_i x$$

$$At \quad x = -1 \qquad y = B_i - 1$$

$$x = -\frac{1}{B_i} \qquad y = 0$$

Substituting the above values to equation (4.50), I_1 becomes

$$I_1 = -\frac{1}{B_i^2} e^{-\frac{\lambda}{B_i}} K_1 \int_{B_i-1}^{0} e^{\frac{\lambda}{B_i} y} erf\ \{y\sqrt{\gamma_e}\}dy + \frac{K_2}{B_i} \int_{B_i-1}^{0} erf\ \{y\sqrt{\gamma_e}\}dy \qquad (4.51)$$

Applying equation (4.49) to the first term of equation (4.51), and (4.26) to the second term. I_1 becomes

$$I_1 = -\frac{K_1}{\lambda} e^{-\frac{\lambda}{B_i}} \left[e^{(\frac{\lambda}{B_i})y} erf\ \{y\sqrt{\gamma_e}\} - e^{\frac{\lambda^2}{4B_i}} erf\left\{ y\sqrt{\gamma_e} - \frac{\lambda}{2B_i\sqrt{\gamma_e}} \right\} \right]_{B_i-1}^{0}$$

$$+ \frac{K_2}{B_i\sqrt{\gamma_e}} \left[y\, erf\ \{y\} + \frac{1}{\sqrt{\pi}} e^{-y^2} \right]_{B_i-1}^{0} \qquad (4.52)$$

Expanding and re-arranging (4.52), I_1 becomes

$$I_1 = -\frac{K_1}{\lambda} e^{-\frac{\lambda}{B_i}} erf\{(B_i-1)\sqrt{\gamma_s}\} - \frac{(B_i-1)}{B_i} K_2 erf\{(B_i-1)\sqrt{\gamma_s}\}$$

$$+ \frac{K_1}{\lambda} e^{\frac{\lambda^2}{4B_i^2\gamma_s}} \left[erf\left\{\frac{\lambda}{2\sqrt{\gamma_s}}\right\} + erf\left\{\frac{(B_i-1)\gamma_s + \frac{\lambda}{2B_i}}{\sqrt{\gamma_s}}\right\}\right]$$

$$+ \frac{K_2}{B_i\sqrt{\gamma_s}} \left[1 - e^{(B_i-1)^2\gamma_i^2}\right] \qquad (4.53)$$

Expression I_2 of equation (4.48) is

$$I_2 = -\int_{-\frac{1}{B_i}}^{+1} erf\{(1+B_i x)\sqrt{\gamma_s}\}(K_1 e^{\lambda|x|} - K_2)dx$$

$$\int_{-\frac{1}{B_i}}^{0} K_1 erf\{(1+B_i x)\sqrt{\gamma_s}\} e^{-\lambda|x|} dx - K_1 \int_{0}^{1} erf\{(1+B_i x)\sqrt{\gamma_s}\}dx$$

$$+ K_2 \int_{-\frac{1}{B_i}}^{+1} erf\{(1+B_i x)\sqrt{\gamma_s}\}dx \qquad (4.54)$$

$$Let \quad y = 1+B_i x \qquad dy = B_i dx$$

$$At \quad x = 1 \qquad y = B_i+1$$

$$x = -\frac{1}{B_i} \qquad y = 0$$

Substituting the above values into (4.54), I_2 becomes

$$I_2 = -\frac{K_1}{B_i} e^{-\frac{\lambda}{B_i}} \int_0^1 erf\{y\sqrt{\gamma_s}\} e^{\frac{\lambda}{B_i} y}\, dy - \frac{K_1}{B_i} e^{\frac{\lambda}{B_i}} \int_1^{B_i+1} erf\{y\sqrt{\gamma_s}\} e^{-\frac{\lambda}{B_i} y}\, dy$$

$$+ \frac{K_2}{B_i} \int_0^{B_i+1} erf\{y\sqrt{\gamma_s}\}\, dy \qquad (4.55)$$

Applying equation (4.49) to the first and and second term of (4.55), and (4.26) to the third term, equation (4.54) then becomes

$$I_2 = -\frac{K_1}{\lambda} e^{\frac{\lambda}{B_i}} \left[e^{\frac{\lambda}{B_i} y} erf\{y\sqrt{\gamma_s}\} - e^{\frac{\lambda^2}{4B_i^2\gamma_s}} erf\left\{ y\sqrt{\gamma_s} - \frac{\lambda}{2B_i\sqrt{\gamma_s}} \right\} \right]_0^1$$

$$+ \frac{K_1}{\lambda} e^{\frac{\lambda}{B_i}} \left[e^{-\frac{\lambda}{B_i} y} erf\{y\sqrt{\gamma_s}\} - e^{\frac{\lambda^2}{4B_i^2\gamma_s}} erf\left\{ y\sqrt{\gamma_s} + \frac{\lambda}{2B_i\sqrt{\gamma_s}} \right\} \right]_1^{B_i+1}$$

$$+ \frac{K_2}{B_i\sqrt{\gamma_s}} \left[y\, erf\{y\sqrt{\gamma_s}\} + \frac{1}{\sqrt{\pi}} e^{-y^2\gamma_s} \right]_0^{(B_i+1)\gamma_s} \qquad (4.56)$$

Expanding and re-arranging (4.56), I_2 becomes

$$I_2 = -\frac{K_1}{\lambda} erf\{\sqrt{\gamma_s}\} + \frac{K_1}{\lambda} e^{\frac{\lambda^2}{4B_i^2\gamma_s}} erf\left\{ \frac{\gamma_s - \frac{\lambda}{2B_i}}{\sqrt{\gamma_s}} \right\}$$

$$- \frac{K_1}{\lambda} e^{\frac{\lambda^2}{4B_i^2\gamma_s}} erf\left\{ \frac{\lambda}{2B_i^2\gamma_s} \right\} + \frac{K_1}{\lambda} e^{-\lambda} erf\{(B_i+1)\sqrt{\gamma_s}\}$$

$$- \frac{K_1}{\lambda} e^{\frac{\lambda^2}{4B_i^2\gamma_s}} erf\left\{\frac{(B_i+1)+\frac{\lambda}{2B_i}}{\sqrt{\gamma_s}}\right\} - \frac{K_1}{\lambda} erf\{\sqrt{\gamma_s}\}$$

$$+ \frac{K_1}{\lambda} e^{\frac{\lambda^2}{4B_i^2\gamma_s}} erf\left\{\frac{\gamma+\frac{\lambda}{2B_i}}{\sqrt{\gamma_s}}\right\} + \frac{(B_i+1)}{B_i} K_2 erf\{(B_i+1)\sqrt{\gamma_s}\}$$

$$+ \frac{K_2}{B_i\sqrt{\gamma_s\pi}}\left[e^{(B_i+1)^2\gamma_s} - 1\right] \qquad (4.57)$$

Combining equation (4.53) and (4.57), the final expression of T_i is

$$T_i = \left[1 + I_1 + I_2\right]$$

$$= 1 + K_N erf\{(B_i-1)\sqrt{\gamma_s}\} + K_O erf\{(B_i-1)\sqrt{\gamma_s}\}$$

$$- \frac{K_1}{5} erf\{\sqrt{\gamma_s}\} + K_P\left(erf\{K_Q\} + erf\{K_R\}\right)$$

$$+ K_S\left(erf\{K_T\} - erf\{K_U\}\right)$$

$$+ \frac{K_2}{B_i\sqrt{\gamma_s\pi}}\left(e^{-(B_i+1)^2\gamma_s} - e^{-(B_i-1)^2\gamma_s}\right) \qquad (4.58)$$

From equation (4.21), the probability of symbol error is

$$P_{M,MPF} = 2\left(1-\frac{1}{\sqrt{M}}\right)\sum_{all\ i} P[B_i]\left[1 + K_N\, erf\{(B_i-1)\sqrt{\gamma_s}\} + K_Q\, erf\{(B_i-1)\sqrt{\gamma_s}\}\right]$$

$$-2\left(1-\frac{1}{\sqrt{M}}\right)\sum_{all\ i} P[B_i]\left[\frac{K_1}{5} erf\{\sqrt{\gamma_s}\} + K_P\left(erf\{K_Q\} + erf\{K_R\}\right)\right]$$

$$+2\left(1-\frac{1}{\sqrt{M}}\right)\sum_{all\ i} P[B_i]\left[K_S\left(erf\{K_T\} - erf\{K_U\}\right)\right] \qquad (4.59)$$

where

$$K_P = \frac{K_1 e^{\frac{\lambda^2}{4B_i^2\gamma_s}}}{\lambda} \qquad K_S = \frac{K_1}{5} e^{\frac{\lambda}{B_i}} e^{\frac{\lambda^2}{4B_i\gamma_s}}$$

$$K_Q = \frac{\gamma_s - \frac{\lambda}{2B_i}}{\sqrt{\gamma_s}} \qquad K_T = \frac{\gamma_s + \frac{\lambda}{2B_i}}{\sqrt{\gamma_s}}$$

$$K_R = \frac{(B_i-1)\gamma_s + \frac{\lambda}{2B_i}}{\sqrt{\gamma_s}} \qquad K_U = \frac{(B_i+1)\gamma_s + \frac{\lambda}{2B_i}}{\sqrt{\gamma_s}}$$

4.4 Illustrative Results for 16, 64 and 256-QAM

The expression given in sections 4.3.2, 4.3.3 and 4.3.4 can be used to derive the probability of symbol error for any M-ary QAM scheme by simply changing the value of M in equation (4.21). For illustrative purposes, three widely used modulation schemes 16, 64 and 256-QAM were considered in this section. The performance curves for these modulation schemes under various multipath fading conditions are shown in Figures 4.2, 4.3 and 4.4.

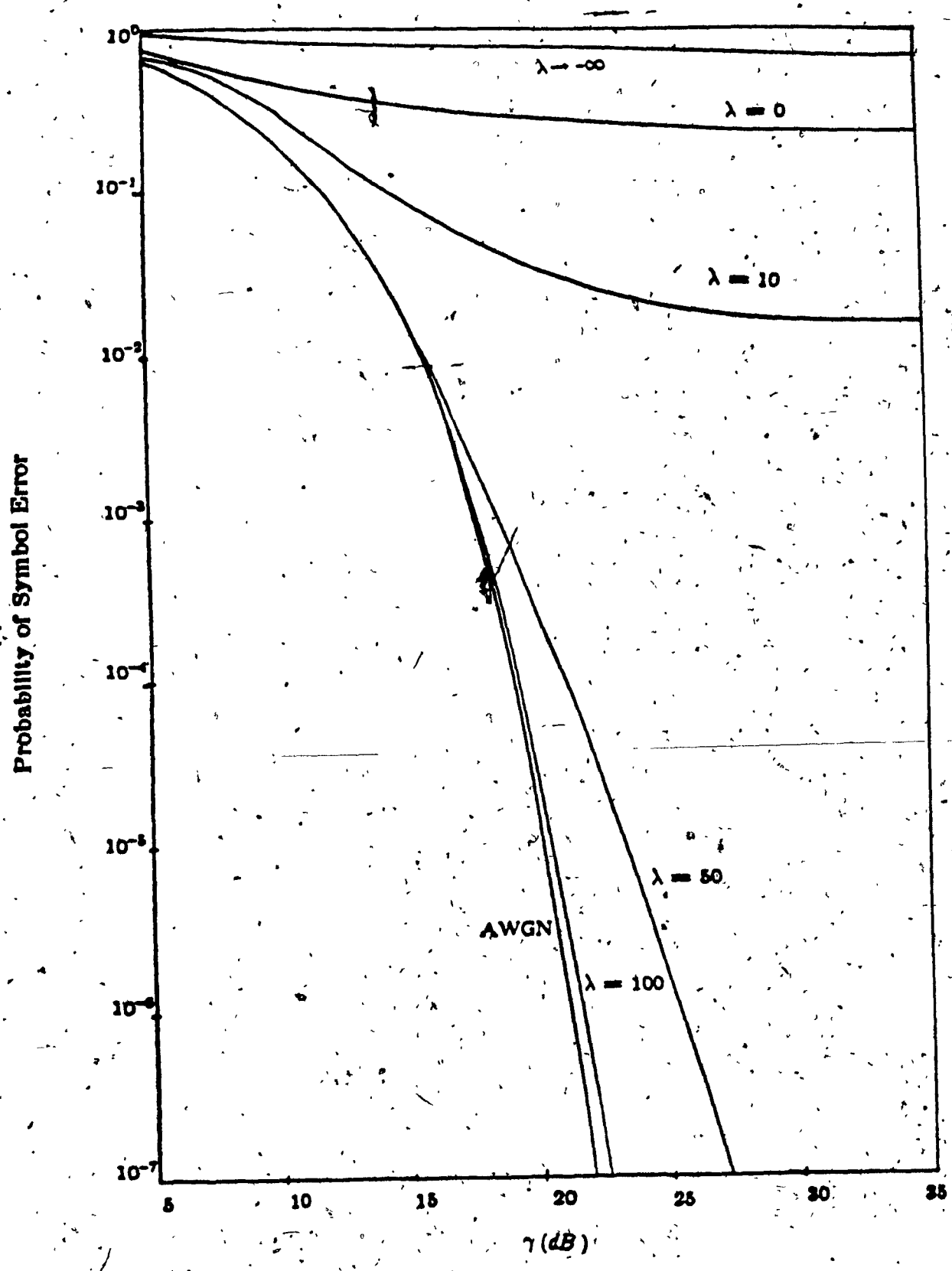

Figure 4.2 The probability of symbol error of a 16-QAM system.

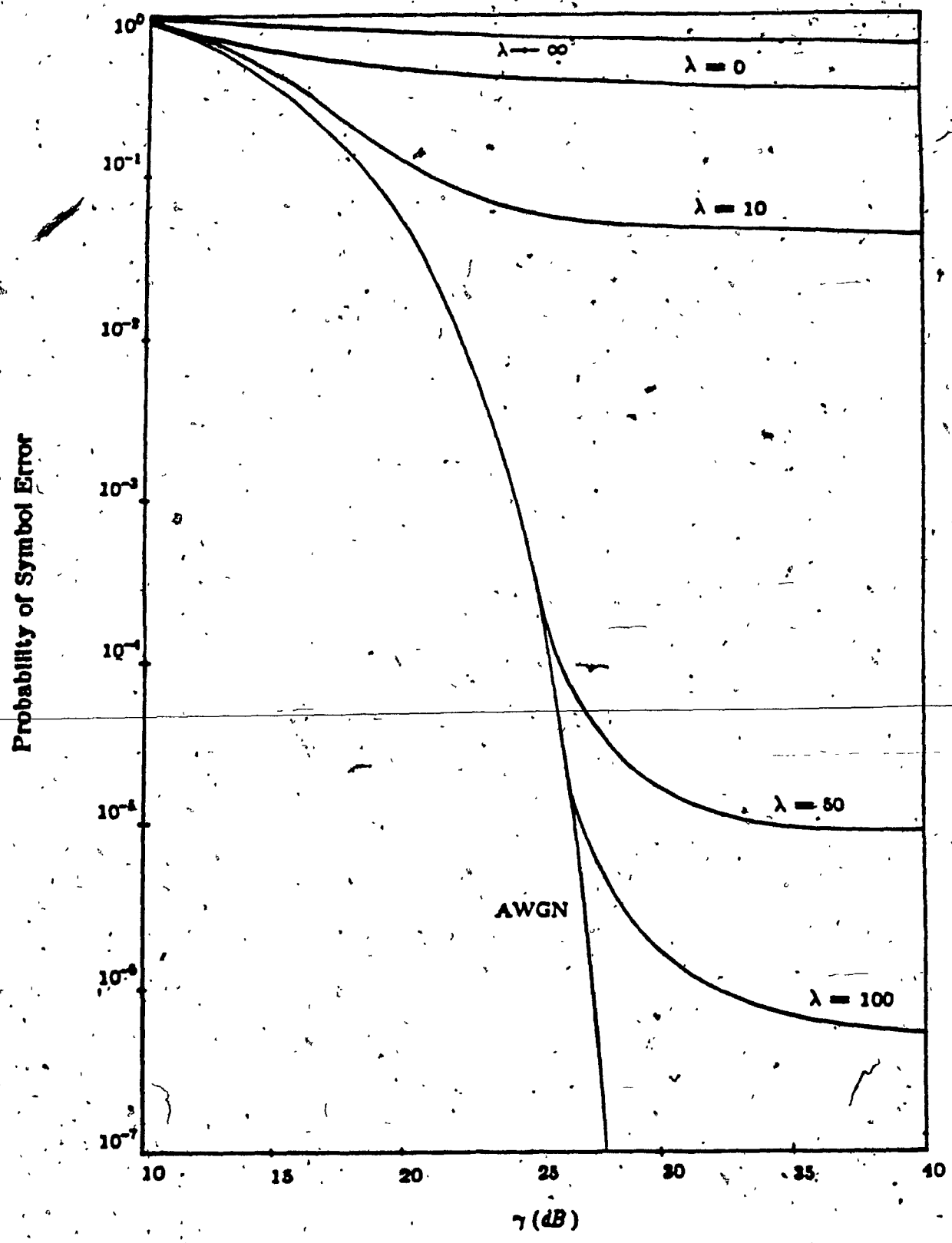

Figure 4.3 The probability of symbol error of a 64-QAM system.

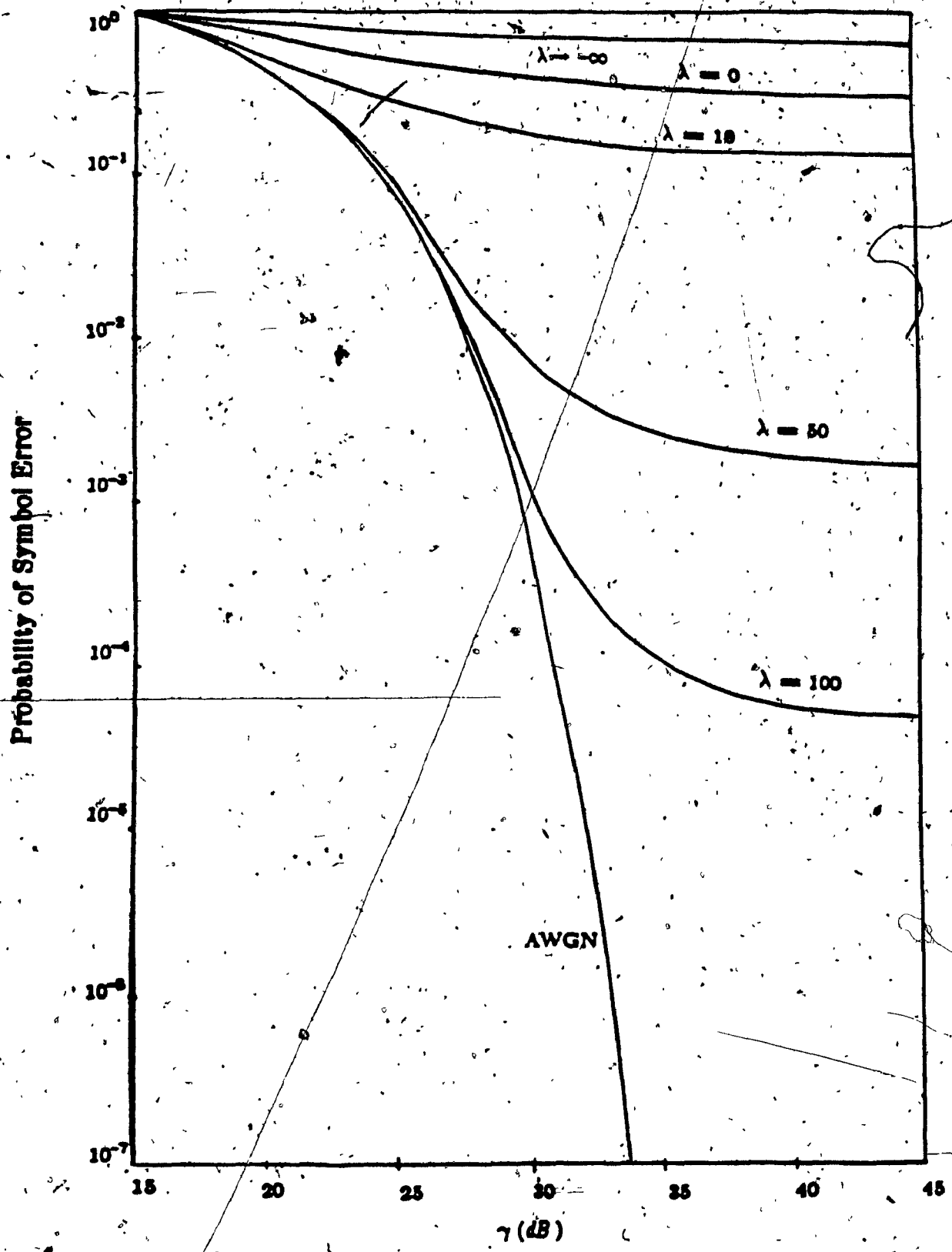

Figure 4.4 The probability of symbol error of a 256-QAM system.

At The Negative Extreme Value $\lambda \rightarrow -\infty$

For all illustrative results, the worst case occurs at $\lambda \rightarrow -\infty$, and the probabilities of error are very high. It is shown that increasing the power or E_s/N_0 cannot provide a better performance. In practice, this corresponds to the situation when the direct and the reflected rays are almost equal in amplitude but opposite in phase, thus canceling each other at the receiver to produce a deep fade phenomenon in most of the time.

At The Middle Value $\lambda = 0$

The performance improvements of 16, 64, 256-QAM schemes are not very impressive. The symbol error rate $P_{M,MPF}$ of each modulation system is still very high, i.e., the channel is heavily distorted.

At The General Values of $\lambda = 10, 50$, and 100

The values of λ equal 10, 50 and 100 were chosen to be the general values to represent the different fading conditions. It should be mentioned that in a microwave digital system, a probability of symbol error of 10^{-3} is a tolerable value. With this in mind and from the performance curves of Figures 4.1, 4.2, and 4.3, it is apparent that with $\lambda = 10$, the system performance is very poor and not acceptable for three cases, 16, 64, and 256-QAM systems. As fading conditions become milder, i.e., λ equals 50 and 100 respectively, the system performance is better.

The results also show that for the same fading condition, i.e., same value of λ, the higher the modulation level M, the worse the performance. For example, when λ equals 100, the performance of 16-QAM in an MPF channel is close to that in an AWGN environment, while the performance curve of 256-QAM is still worse staying at $8 * 10^{-5}$ for high E_s/N_0.

It has been shown that multipath fading has a significant impact in the M-ary QAM microwave radio. Under the same fading condition, the effects on the system performance become more severe as the modulation level increases (Figures 4.1, 4.2 and 4.3). The higher level QAM is more vulnerable to MPF distortion. In addition, the receiver has to detect more signal states with the added complexities from phase jitter and timing problem. Therefore, in order to achieve high transmission capacity at the higher modulation level, it is necessary to use fading countermeasuring techniques such as diversity, equalization and FEC to recover the transmission objectives.

CHAPTER V

CONCLUSIONS AND SUGGESTIONS FOR FURTHER RESEARCH

5.1 Conclusions

The performance of an M-ary QAM signal in a line-of-sight MPF channel has been introduced and investigated.

To investigate the MPF phenomenon, several well established models were used to represent the fading effect. Each model has certain specific features that characterize the effects of MPF. Of the four investigated models, it was shown that the two-path and the simplified three-path models are the most popular ones. These two models provide mathematical simplicity at the expense of marginal accuracy.

The two-path model and a recent postulated PDF were used to evaluate the probability of symbol error for M-ary QAM. It was shown that this PDF model can be used to analyze many different fading situations. This is done simply by changing the value of the parameter λ. The fading conditions under investigation can range from no MPF to the worst MPF condition.

The probability of symbol error of 16, 64 and 256-QAM were evaluated for normal and different fading conditions as illustrative examples. It was shown that MPF has a significant impact on the performance of M-ary QAM systems. As the modulation level increases, the waveform distortion become more severe, and hence the performance is heavily degraded.

The effects of MPF cannot be overcome by simply increasing the transmission power. Therefore, countermeasuring techniques such as diversity, equalization and FEC are needed in order to achieve the performance objectives.

5.2 Suggestions For Further Research

Although the performance of M-ary QAM in an MPF channel was extensively studied, there are certainly some other interesting aspects which can be further investigated. The following topics are suggested as an extension of the work presented here.

1. Relationship between λ and physical phenomenon

In the mathematical analysis, λ is a parameter that represents the degree of MPF. The severity of fading phenomenon can be varied by changing the value of λ. Therefore, it is interesting to relate the parameter λ to the actual physical fading phenomenon.

2. Effects of MPF On Carrier And Symbol Timing Recovery System

In a coherent communication system, carrier recovery and timing recovery processes are required in the receiver. No matter how effective a digital receiver in performing these tasks under normal propagation conditions, in an MPF channel, these recovery processes are distorted. As a result, this can considerably degrade the performance of the transmission system. Hence, the analysis of the effect of carrier and timing recovery in an MPF channel is useful.

3. Countermeasuring Techniques And Performance

Various countermeasuring techniques to combat the effect of MPF have been reviewed. Since M-ary QAM has become a popular modulation scheme due to its bandwidth efficiency, it is useful to study the performance of these techniques associated with various levels of QAM signals in different fading distorted conditions.

REFERENCES

[1] D.P. Tayor and P.R. Hartmann, "Telecommunications by Microwave Digital Radio," *IEEE Communications Mag.* , vol.24, no.8, pp.11-16, August 1986.

[2] C.A. Siller, "Multipath Propagation," *IEEE Communications Mag.* , vol. 22, no. 2, pp.6-15, February 1984.

[3] E.W. Allen, "The Multipath Phenomenon in Line-of-Sight Digital Transmission Systems," *Microwave Journal* ,pp.215-225, May 1984.

[4] G.M. Babler, "A Study of Frequency Selective Fading for a Microwave Line-of-Sight Narrowband Radio Channel," *The Bell System Technical Journal* , vol.51, no.3, pp.731-757, March 1972.

[5] J.A. Brana, "*Multipath Fading : Channel Characterization and Performance of PSK systems*," Master Thesis, Concordia University, Electrical Engineering Department, April 1986.

[6] J.A. Brana, T. Le-Ngoc, and V.K. Bhargava, "Performance of PSK Systems in a Line-of-Sight Multipath Fading Channel," *IEEE Montech* , pp.222-230, Montreal 1986.

[7] C.L. Ruthroff, "Multipath Fading on Line-of-Sight Microwave Radio Systems as a Function of Path Length and Frequency," *The Bell Technical Journal*, vol. 50, no. 7, pp.2375-2398, September 1971.

[8] W.T. Barnett, "Multipath Propagation at 4, 6, and 11 GHz," *The Bell System Technical Journal*, vol. 51, no.2, pp.321-360, February 1972.

[9] W.D. Rummler, "A Multipath Channel Model for Line-of-Sight Digital Radio Systems," *IEEE International Conference on Communications* , pp. 47.5.1-47.5.4, Toronto 1978.

[10] L.J. Greenstein and B.A. Czekaj, "A Polynomial Model for Multipath Fading Channel Responses," *The Bell System Technical Journal*, vol. 59, no. 7, pp.1197-1225, September 1980.

[11] W.C. Jakes Jr., "An Approximate Method to Estimate an Upper Bound on the Effect of Multipath Delay Distortion on Digital Transmission," *IEEE International Conference on Communications*, pp.47.1.1-47.1.5, Toronto 1978.

[12] L.J. Greenstein and V.K. Prabhu, "Analysis of Multipath Outage with Applications to 90-Mbit/s PSK Sytems at 6 and 11 Ghz.," *IEEE International Conference on Communications*, pp.47.2.2-47.2.5, Toronto 1978.

[13] N.Amitay and L.J. Greentein, "Multipath Outage Performance of Digital Radio Receivers Using Finite-Tap Adaptive Equalizers," *IEEE Transactions on Communications*, vol. CS-32, no.5, pp. 597-608, May 1984.

[14] T. Aulin, "Characteristics of a Digital Mobile Radio Channel," *IEEE Transactions on Vehicular Technology*, vol. VT-30, no. 2, pp. 45-53, May 1981.

[15] J.G. Proakis, *Digital Communications*, McGraw-Hill Company,1983.

[16] M. Emshwiller, "Characterization of The Performance of PSK Digital Radio Transmission in The Presence of Multipath Fading," *IEEE International Conference on Communications*, pp.47.3.1-47.3.6, Toronto 1978.

[17] W.D. Rummler, R.P. Coutts, M. Liniger, "Multipath Fading Channel Models for Microwave Digital Radio," *IEEE Communications Mag.*, vol. 24, no. 11, pp. 30-41, November 1986.

[18] P.A. Bello, "Characterization of randomly time variant linear channels," *IEEE Trans.on Comm.*, vol. CS-11, no. 4, pp. 360-393, December 1963.

[19] D.R. Smith and J.J. Cormack, "Measurements and characterization of a multipath fading channel for application to digital radio links," *IEEE International Conference on Communications* , pp. 4.1-4.6, 1982.

[20] H. Yamamoto, "Advanced 16-QAM Techniques for Microwave Digital Radio," *IEEE Communications Mag.* , vol. 24, no. 2, pp. 36-45, February 1986.

[21] J.K. Chamberlain et al, "Receiver Techniques for Microwave Digital Radio," *IEEE Communications Mag.* , vol. 24, no. 11, pp. 43-54, November 1986.

[22] S. Qureshi, "Adaptive Equalization," *IEEE Communications Mag.*, vol. 20, no.3, pp 9-16, March 1982.

[23] K.S:Shanmugan,*Digital and Analog Communication Systems*, John Wiley & Sons, Inc. 1979.

[24] W.K. Wong, "Adaptive Transversal Filters for Multipath Compensation in Microwave Digital Radio," International Conference on Communications ,pp. 989-992, Amsterdam 1984.

[25] D.R. Hummel and F.W. Ratcliffe, "Calculation of Error Probability for MSK and OQPSK Systems Operating in a Fading Multipath Environment," *IEEE Transactions on Vehicular Technology*, vol. VT-30, no. 3, pp.112-120, August 1981.

[26] L.B. Milstein et al, "Comparison of Performance of 16-ary QASK and MSK Over a Frequency Selective Rician Fading Channel," *IEEE Transactions on Communications*, vol. CS-29, no. 11, November 1981.

[27] S.G. Wilson, "Different Phase-Shift Keying Performance on L-Band Aeronautical Satellite Channels: Test Results and a Coding Evaluation," *IEEE Transactions on Communications*, vol. CS-24, no.3, pp.374-380, March 1976.

[28] H.D. Chadwick, "The Error Probability of a Wide-Band FSK Receiver in the Presence of Multipath Fading," *IEEE Transaction on Communications*, vol. CS-19, no.5, pp.699-706, October 1971.

[29] R.W. Lucky, J. Saltz, and E.J. Weldon, Jr., *Principle of Data Communications*, McGraw-Hill Book Company, 1966.

[30] A. Papoulis *Probability, Random Variables and Stochastic Processes*, Second Edition, McGraw-Hill Book Company, 1984.

[31] M. Abramowitz and L.A. Stegun, *Handbook of Mathematical Functions*, nineth Edition, United-States Department of Commerce, 1970.